



Chloroplasts lacking class I glutaredoxins are functional but show a delayed recovery of protein cysteinyl redox state after oxidative challenge

Finja Bohle^{a,b}, Jacopo Rossi^c, Sadia S. Tamanna^a, Hannah Jansohn^a, Marlene Schlosser^a, Frank Reinhardt^d, Alexa Brox^e, Stephanie Bethmann^f, Stanislav Kopriva^g, Oliver Trentmann^a, Peter Jahns^f, Marcel Deponte^h, Markus Schwarzländerⁱ, Paolo Trost^c, Mirko Zaffagnini^c, Andreas J. Meyer^b, Stefanie J. Müller-Schüssele^{a,*}

^a Molecular Botany, Department of Biology, RPTU Kaiserslautern-Landau, D-67633, Kaiserslautern, Germany

^b Chemical Signalling, Institute of Crop Science and Resource Conservation (INRES), University of Bonn, D-53113, Bonn, Germany

^c Department of Pharmacy and Biotechnology, University of Bologna, I-40126, Bologna, Italy

^d Plant Physiology, Department of Biology, RPTU Kaiserslautern-Landau, D-67633, Kaiserslautern, Germany

^e Crop Functional Genomics, Institute of Crop Science and Resource Conservation (INRES), University of Bonn, D-53113, Bonn, Germany

^f Plant Biochemistry, Heinrich-Heine-University Düsseldorf, D-40225, Düsseldorf, Germany

^g Institute for Plant Sciences, Cluster of Excellence on Plant Sciences (CEPLAS), University of Cologne, Cologne, 50674, Germany

^h Biochemistry, Department of Chemistry, RPTU Kaiserslautern-Landau, D-67633, Kaiserslautern, Germany

ⁱ Institute of Plant Biology and Biotechnology, University of Münster, D-48143, Münster, Germany

ARTICLE INFO

Keywords:

Glutaredoxin

GRXC5

S-glutathionylation

Redox-sensitive GFP

E_{GSH}

Genetically encoded biosensor

Photosynthesis

Plastid

Glutathione

ABSTRACT

Redox status of protein cysteinyl residues is mediated via glutathione (GSH)/glutaredoxin (GRX) and thioredoxin (TRX)-dependent redox cascades. An oxidative challenge can induce post-translational protein modifications on thiols, such as protein S-glutathionylation. Class I GRX are small thiol-disulfide oxidoreductases that reversibly catalyse S-glutathionylation and protein disulfide formation. TRX and GSH/GRX redox systems can provide partial backup for each other in several subcellular compartments, but not in the plastid stroma where TRX/light-dependent redox regulation of primary metabolism takes place. While the stromal TRX system has been studied at detail, the role of class I GRX on plastid redox processes is still unknown. We generate knockout lines of *GRXC5* as the only chloroplast class I GRX of the moss *Physcomitrium patens*.

While we find that PpGRXC5 has high activities in GSH-dependent oxidoreductase assays using hydroxyethyl disulfide or redox-sensitive GFP2 as substrates *in vitro*, $\Delta grxc5$ plants show no detectable growth defect or stress sensitivity, in contrast to mutants with a less negative stromal E_{GSH} ($\Delta gr1$). Using stroma-targeted roGFP2, we show increased protein Cys steady state oxidation and decreased reduction rates after oxidative challenge in $\Delta grxc5$ plants *in vivo*, indicating kinetic uncoupling of the protein Cys redox state from E_{GSH} . Compared to wildtype, protein Cys disulfide formation rates and S-glutathionylation levels after H_2O_2 treatment remained unchanged. Lack of class I GRX function in the stroma did not result in impaired carbon fixation.

Our observations suggest specific roles for GRXC5 in the efficient transfer of electrons from GSH to target protein Cys as well as negligible cross-talk with metabolic regulation via the TRX system. We propose a model for stromal class I GRX function in efficient catalysis of protein dithiol/disulfide equilibria upon redox steady state alterations affecting stromal E_{GSH} and highlight the importance of identifying *in vivo* target proteins of GRXC5.

1. Introduction

Oxygenic photosynthesis has shaped our planet by increasing oxygen levels in the atmosphere, and by enabling solar-driven carbon fixation. In phototrophic eukaryotic life forms, former free-living cyanobacteria

now serve as chloroplasts in light-harvesting and production of reducing equivalents to power reductive processes in cell metabolism [1]. Land plant chloroplasts face multiple oxidative challenges as environmental conditions such as light intensity, water availability and temperature can rapidly fluctuate and cause imbalances between light reactions and

* Corresponding author. Rheinland-Pfälzische Technische Universität Kaiserslautern-Landau (RPTU), Erwin-Schrödinger-Str. 70, 67663, Kaiserslautern, Germany.
E-mail address: mueschue@rptu.de (S.J. Müller-Schüssele).

carbon fixation. Plants have adapted to a frequently changing environment by evolving mechanisms to regulate photochemistry and carbon fixation in a matter of minutes, as well as mechanisms to acclimate to a changed steady state in a matter of hours or days [2–5]. Regulation of the enzymatic reactions of the Calvin-Benson-Bassham cycle (CBB cycle) to match the activity of the light reactions guarantees efficient re-oxidation of the electron acceptor of light reactions, NADP^+ , and avoids futile cycling under dark conditions when the oxidative pentose phosphate pathway is active [6]. Thus, many stromal enzymes evolved Cys-based redox-regulation [7,8]. This regulation of protein activity or oligomerization [9] can be mediated by post-translational changes in cysteinyl thiol redox states, including the formation/reduction of regulatory disulfide bonds on target proteins [10–12]. The thioredoxin (TRX) system derives electrons from the photosynthetic electron transport (PET) or NADPH for the reduction of specific regulatory disulfides on metabolic enzymes [13]. The redox state of these thiol-switches depends on the redox state of TRXs, which in turn depend on PET/NADPH-dependent reduction rates [14,15] and oxidation rates [16]. TRX oxidation rates can be linked via 2 Cys-peroxiredoxins (PRX) to the detoxification of hydrogen peroxide (H_2O_2) [17–19] which functions as terminal electron acceptor.

When the stromal NADP pool becomes increasingly reduced, generation of reactive oxygen species (ROS) increases (photoinhibitory conditions) as photosystem I (PSI) becomes acceptor-limited [2]. Via superoxide dismutases, superoxide is rapidly (without input of additional electrons) converted to H_2O_2 that can react with cysteine residues causing thiol oxidation, either directly (highly reactive Cys only) or via the Cys-redox relays [20,21]. To balance ROS formation and repair ROS-induced oxidative damage, chloroplasts have evolved multiple detoxification and repair systems that either draw electrons from the TRX system or the glutathione system.

Glutathione (GSH) is a cysteine-containing tri-peptide present at millimolar concentrations in the cytosol and chloroplast stroma serving multiple roles in cellular metabolism and defense [22,23]. First, glutathione is an important electron donor for H_2O_2 detoxification or repair of ROS-induced damages (reviewed in [24] and Müller-Schüssele et al. [25]). Second, it can form mixed disulfides with cysteinyl residues in proteins (protein S-glutathionylation), either as a consequence of cysteine oxidation by H_2O_2 (S-sulfenylation), or enzymatically catalysed by class I glutaredoxins (GRXs) (Fig. 1) [20]. Class I GRXs are small oxidoreductases belonging to the TRX superfamily, that can form or release protein S-glutathionylation and disulfides [26–29]. In contrast to animal cells, no glutathione S-transferase-dependent protein (de)glutathionylation activity has been described in plants [30,31]. S-glutathionylation can affect protein activity and/or oligomerization as well as act as a protection against protein Cys over-oxidation, depending on the modified protein and site [32–35]. GRXs and TRXs can at least partially functionally complement each other, lack of both activities in the cytosol

leads to lethality in *S. cerevisiae* [36]. Thus, the redox state of individual cysteine residues depends on an intricate network of redox reactions with partially overlapping but also specific roles for TRX- and GSH/GRX-dependent reactions.

In the plastid stroma, the presence of a glutathione reductase (GR) leads to a highly reducing steady-state glutathione redox potential (E_{GSH}) with only nanomolar amounts of oxidized glutathione, glutathione disulfide (GSSG) (Fig. 1) [37–40]. Stromal steady-state E_{GSH} monitored by the genetically encoded biosensor Grx1-roGFP2 [41–43] revealed light-dependent redox dynamics [40,44].

In contrast to mitochondria and cytosol, the plastid TRX system does not constitute an effective functional backup system for the stromal GSH/GRX system, as a lack in stromal GR causes embryo-lethality in *A. thaliana* [39,45]. In the model moss *Physcomitrium patens*, plants lacking mitochondria/plastid-targeted glutathione reductase (PpGR1) had a shifted (less negative) stromal E_{GSH} and were viable, albeit dwarfed and light-sensitive [40]. Plant class I GRX clades that contain isoforms targeted to different subcellular compartments are evolutionary conserved from bryophytes to flowering plants [25]. In the model flowering plant *A. thaliana*, two plastid-targeted class I GRXs exist that differ by the number of cysteines in the active site. While AtGRXS12 contains a single cysteine (WCSYS active site), AtGRXC5 contains two cysteines (YCPYC active site) [25,46]. According to previous phylogenetic analysis, GRXC5 represents the ancestral type of plastid-targeted class I GRX with a single isoform of GRXC5 in the model moss *P. patens* [25].

The chloroplast stroma has been described as a ‘redox battle ground’ [47] of which we are still lacking a functional map. In particular, the roles of glutathione, class I GRX and protein S-glutathionylation are largely uncharted. It is an open question how class I GRX function and S-glutathionylation dynamically interact with the known thiol-switching cascades in the crucial light/dark regulation of chloroplast metabolism.

Here, we set out to understand the role of class I GRX in the stromal redox network of plants. To this end we generated plant lines lacking class I GRX activity in the stroma, by exploiting the fact that only a single plastid-targeted class I GRX is present in *Physcomitrium patens*. We combine biochemical characterization of PpGRXC5 *in vitro* with *in vivo* biosensing using stroma-targeted roGFP2 to dynamically monitor protein Cys redox changes after oxidative challenge.

2. Material and methods

2.1. *In vitro* analyses of PpGRXC5

For recombinant protein expression of PpGRXC5, *P. patens* cDNA was used to amplify GRXC5 without targeting peptide (starting at the Ala 120 codon) using the primer combination PpGRXC5_A120_F

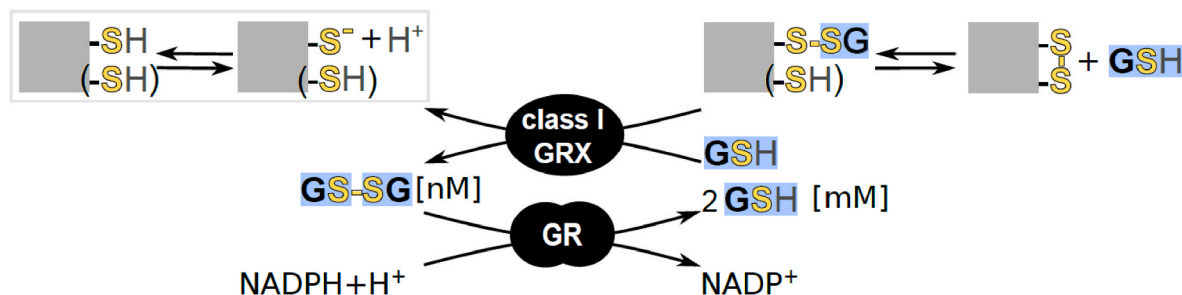


Fig. 1. Scheme of class I GRX and glutathione reductase function. Class I glutaredoxins (GRX) can reversibly modify cysteinyl residues (thiol group SH, thiolate S^-) in proteins by forming a mixed disulfide with the tripeptide glutathione (GSH). If a second cysteine is present in a suitable distance, this S-glutathionylation can be released by intramolecular disulfide formation, as observed for the genetically encoded redox sensor roGFP2. Glutathione reductase (GR) uses NADPH to reduce glutathione disulfide (GSSG) yielding two molecules of reduced glutathione (GSH). The resulting low steady-state glutathione redox potential E_{GSH} is then used by GRX to maintain a high steady-state thiol:disulfide ratio for most cysteinyl residues. Grey squares represent GRX substrate proteins, black rounded shapes enzymes.

GGGGACAAGTTGTACAAAAAGCAGGCTTAGCAGCAGGTT CGGGG and PpGrxC5_cds_R GGGGACCACCTTTGTACAAGAAAGCTGGGTG TCA ACTCTGTTTGCACCAG, adding *attB1* and *attB2* sites. The PCR-product was cloned via Gateway™ into pDONR207, verified by sequencing, and subsequently inserted into the pETG-10A vector. Recombinant proteins (roGFP2 [41], PpGRXC5, AtGRXC1 (AT5G63030 [48]) were purified from transformed *E. coli* strain *Rosetta2* as described in Trnka et al. [29] and Ugalde et al. [49].

2.2. Hydroxyethyl disulfide (HED) assay

De glutathionylation activity of PpGRXC5 was tested according to Zaffagnini et al. [50]. Prior to the assay, the concentration of GRXC5 was determined via Bradford assay [51]. All chemicals were dissolved in 100 mM Tris-HCl pH 7.9. A 20 mM NADPH stock was prepared, and concentration was verified via absorption measurements using the NADPH extinction coefficient of $6.23 \text{ mM}^{-1} \text{ cm}^{-1}$. To test for the GRX concentration in which the GRX shows a linear activity, HED assays were performed in 100 mM Tris-HCl, 1 mM EDTA pH 7.9 using 1 mM GSH and 0.7 mM HED, varying the concentration of the GRX from 10 to 50 nM. The HED assay, with GSH as variable substrate, was performed by preparing a 1 ml cuvette containing 0.5–4 mM GSH and 0.7 mM bis (2-hydroxyethyl)disulfide (HED). With HED as variable substrate, GSH concentration was kept constant at 1 mM, while HED concentrations varied from 0.3 mM to 1.5 mM. To the HED and GSH mixture 200 μM NADPH and 100 mM Tris-HCl 1 mM EDTA pH 7.9 were added. After exactly 3 min of incubation, GR (final concentration of $6 \mu\text{g ml}^{-1}$, *Saccharomyces cerevisiae*, Sigma-Aldrich CAS 9001-48-3, 100–300 units/mg protein) and GRXC5 (final concentration 30 nM) were added to the cuvette adding up to a final volume of 1 ml. For each concentration of varying GSH or HED, a background activity was determined by replacing GRX with buffer (Tris-HCl, pH 7.9). The absorbance decrease at 340 nm was followed for 1 min using a NanoDrop™ 2000c spectrophotometer (Thermo Fisher Scientific).

2.3. roGFP2-based in vitro assays

Oxidation and reduction assays using roGFP2 [41,42,52] were performed in a 96-well plate in a fluorescence plate reader (CLARIOstar® Plus, BMG Labtech). For oxidized and reduced roGFP2 controls, roGFP2 was treated for 30 min with 10 mM DTT or 10 mM H_2O_2 before the assay start. To assess the reduction capacities of PpGRXC5, 1 μM of untreated (oxidized) roGFP2 was pipetted into a well containing 1 μM GRX (PpGRXC5, AtGRXC1), 100 μM NADPH and 1 unit *S. cerevisiae* GR in 100 μl of 100 mM potassium phosphate buffer pH 7.4. After measuring for 10 cycles, a final concentration of 2 mM GSH was added automatically by the injection needles of the plate reader into the respective wells. Fluorescence was followed until roGFP2 ratio stabilized. For assessing oxidation capacities of PpGRXC5, 10 μM roGFP2 was pre-reduced with 10 mM DTT for 30 min and subsequently desalted via Zeba™ Spin Desalting Columns (ThermoFisher) following the manufacturer's instructions. 1 μM of pre-reduced roGFP2 was mixed with 1 μM of PpGRXC5 or AtGRXC1 in potassium phosphate buffer pH 7.4. Two mM GSSG was added via the injection needles of the plate reader after 5 min of initial measurements and the measurement continued until roGFP2 ratio stabilized. Fluorescence intensities were collected by excitation at 390–10 nm or 480–10 nm and emission at 530–10 nm.

2.4. Plant materials and growth conditions

Physcomitrium patens (Hedw.) Bruch & Schimp ecotype 'Gransden 2004' (International Moss Stock Centre (IMSC, <http://www.moss-stock-center.org>), accession number 40001) was grown axenically and regularly sub-cultured in agitated liquid medium (KNOP medium: 250 mg l^{-1} KH_2PO_4 , 250 mg l^{-1} KCl, 250 mg l^{-1} $\text{MgSO}_4 \times 7\text{H}_2\text{O}$, 1 g l^{-1} Ca $(\text{NO}_3)_2 \times 4\text{H}_2\text{O}$ and 12.5 mg l^{-1} $\text{FeSO}_4 \times 7\text{H}_2\text{O}$, pH 5.8) [53]

supplemented with micro-elements (ME), (H_3BO_3 , MnSO_4 , ZnSO_4 , KI, $\text{Na}_2\text{MoO}_4 \times 2\text{H}_2\text{O}$, CuSO_4 , $\text{Co}(\text{NO}_3)_2$). For phenotypic analyses, *P. patens* gametophores were grown on KNOP ME agar plates (12 g l^{-1} purified agar; Oxoid, Thermo Scientific, Waltham, MA, USA). Light intensity in growth cabinets was set to 70–100 $\mu\text{mol photons m}^{-2} \text{ s}^{-1}$ and 16:8 h light/dark cycle at 22 °C, if not indicated otherwise.

2.5. Generation of transgenic lines

Δgrxc5. The complete *GRXC5* (Pp3c3_7440V3.3 (V1.6 Pp1s321_10V6.1)) coding sequence (cds) was exchanged via homologous recombination with a *nptII* resistance cassette under the control of the *NOS* promoter and terminator. The knock-out construct was assembled by triple-template PCR [54], using the following primer combinations: upstream (5') homologous region (HR) PpGRXC5ko_5PHR_P1 ATCACAGGAAGCTATGGAAGGCA and PpGRXC5ko_5P_HR_P2 TTGACAGGATCCGATAATCCCACCTTAGCACCAGG, resistance cassette *GRXC5ko_npt_F*: TGCTAAGTGGGGATTATCGGATCCTGTCAAA CACTG and *GRXC5ko_npt_R*: CGTATGTGATGGCATGACAGGAGG CCGGATCTAGTA, downstream (3') HR PpGrxC5ko_3PHR_P3 ATCGG GCCTCCTGTCATGCCATCACATACGGAACCT and PpGrxC5ko_3PHR_P4 ATCTTCAGCTCCTCAGTTCTCTCG (Table S1). *EcoRV* restriction sites were introduced by ligating the triple-template PCR product into the pJET1.2 (Thermo Scientific, Waltham, MA, USA) vector. The resulting vector was amplified in and purified from *E. coli DH5alpha* strain, digested with *EcoRV* and used for polyethylene glycol-mediated protoplast transformation as previously described [55]. Regenerating plants surviving geneticin G418 (12.5 mg l^{-1}) selection for four weeks were further screened via PCR for homologous 5' and 3' integration of the knock-out construct at the target locus using the primer combinations *GrxC5_5P_F* AAGTAGGGAAAAGAGAGCAGC and *H3b_R* CCAAACGTAAACCGCTTGT as well as *NOST_F* GCGCGGTGTCATCTATGTTA and *GrxC5_3P_R* TGTCGTGTGTTCCGACTTCT (Table S1). Absence of transcript on cDNA-level was confirmed using the primer combination *PpGrxC5_RT_F* TTAATCGGCAGGTGTGTGGA and *PpGrxC5_RT_R* AAAAGCTTCTCACGCGCAT (Fig. S1). *Δgrxc5* lines are available from the IMSC under the accession numbers: *Δgrxc5#54* IMSC-Nr. 40954, *Δgrxc5#249* IMSC-Nr. 40955). *Δgr1* lines in *Δgrxc5#54* genetic background were generated and identified as described in Müller-Schüssele et al. [40], see also Fig. S1, Table S1.

Plastid-targeted roGFP2. The construct of plastid-targeted roGFP2 was generated by overlap PCR. Two DNA templates were generated in separate PCR reactions adding *attB1* and *attB2* sites to the 5' and 3' ends, respectively: the plastid transketolase targeting peptide (TKTP) sequence of *N. tabacum* [43,56] was amplified using TKTP_F (GGGGA-CAAGTTTGTACAAAAAGCAGGCTATGGCGTCTTCTTCTCT) and TKTP_roGFP2_R (CCTCGCCCTTGCTCACCAGCGCAGTCTCAGTT), creating an overlap to the roGFP2 coding sequence. Similarly, roGFP2 was amplified with TKTP-roGFP2_F (ACTGAGACTGCGCTGGTGAGCA AGGGCGAGGAG) and roGFP2-attB2_R (GGGACCACCTTTGTACAA-GAAAGCTGGTCTTACTTGTACAGCTCGTCCATG), creating an overlap with the TKTP sequence (Table S1). The overlap PCR product was cloned by Gateway BP reaction in the pDONR207 entry vector. A clone with correct sequence was recombined via LR reaction into an expression vector (*PTA2_Act5_GW*) containing a Gateway *attR1/attR2* cassette between the *PpActin5* promoter and nopaline synthase (*NOS*) terminator, as well as homologous regions for integration at the *P. patens* *PTA2* locus [57,58]. For protoplast transformation, the expression vector was digested with *BspQ1*, cutting at the ends of *PTA2* homologous regions, and co-transformed with a second uncut plasmid containing the *hpt* resistance cassette (pJET1.2 hpt; cds of hygromycin phosphotransferase under the control of *NOS* promoter and terminator). After four weeks of selection on hygromycin (12.5 $\mu\text{g ml}^{-1}$) [59], two transgenic lines expressing plastid-targeted roGFP2 in *Δgrxc5#54* background (lines #17 (IMSC-Nr. 40957) and #21 (IMSC-Nr. 40958)) and one transgenic line in WT background (#20, IMSC-Nr. 40959) were used for further

analyses and are available from the IMSC.

2.6. Confocal laser scanning microscopy

Microscopy was carried out as described in Müller-Schüssele et al. [40] using a LSM780 (attached to an Axio Observer.Z1) (Carl Zeiss, Oberkochen, Germany) with 25x (Plan-Apochromat 25 × /0.8 Imm Korr NA0.8) or 40x (C-Apochromat 40 × /1.2W Korr NA1.2) objective. roGFP2 redox state was monitored by sequential excitation at 405 nm and 488 nm, detecting emission from 508 to 535 nm. Autofluorescence was recorded using excitation at 405 nm and emission detected from 430 to 470 nm. Chlorophyll autofluorescence was monitored after 488 nm excitation at an emission of 680–735 nm. Image intensities and 405/488 nm ratios were calculated per pixel using a custom MATLAB (MathWorks, Natick, MA, USA)-based software [60]. For experiments with dark/light/dark transitions, protonema and gametophores of *TKTP-roGFP2*-expressing transgenic *P. patens* lines WT#20, $\Delta grxc5\#17$ and $\Delta grxc5\#21$ cultured in liquid medium were dark-adapted for at least 45 min. Subsequently, roGFP2 fluorescence was first imaged for 1 min in the dark (without pre-screening), then during illumination from an external light source with c. 100 $\mu\text{mol photons m}^{-2}\text{s}^{-1}$ from a 90° angle for 5 min (every 30 s), followed by a second period of continued imaging in the dark [40].

2.7. In vivo plate reader-based fluorometry

Ratiometric time-course measurements for roGFP2 were conducted using a CLARIOstar® Plus plate reader (BMG Labtech). During *in vivo* time series, roGFP2 signal was detected using a sequential filter-based excitation of 400–10 nm and 482–16 nm, while emission was detected at 530–40 nm. The degree of oxidation of roGFP2 (OxD) was calculated as described in Aller et al. [61]. Protonema culture of *P. patens* expressing *TKTP-roGFP2* was dispersed and transferred to fresh KNOP-ME pH 5.8 media one week prior to measurements. 200 μl of protonema culture were pipetted with a wide cut pipette tip into wells of a 96-well plate. Cultivation media was taken up after the moss settled to the bottom of the plate and substituted by 200 μl of imaging buffer (10 mM MES, 5 mM KCl, 10 mM CaCl_2 , 10 mM MgCl_2 pH 5.8) [62]. To conduct an *in vivo* sensor calibration, the 200 μl imaging buffer were removed with a 100 μl tip and substituted with the same volume of imaging buffer containing either 10 mM H_2O_2 or 5 mM DPS (2, 2'-dipyridyl disulfide) for complete oxidation, and 10 mM dithiothreitol (DTT) for complete reduction.

For H_2O_2 recovery experiments, H_2O_2 in concentrations ranging from 1 to 10 mM were added manually to the wells. After 30 min in the respective H_2O_2 concentration, buffer was exchanged to imaging buffer to follow roGFP2 re-reduction. For H_2O_2 oxidation rate experiments the plate reader was used in “well mode” with a cycle time of 1.55 s. 200 μl of one-week-old protonema culture expressing *TKTP-roGFP2* was transferred into a 96-well plate and pre-reduced using 10 mM DTT in imaging buffer. DTT was removed and substituted with 160 μl imaging buffer. After 60 s H_2O_2 was automatically injected by the plate reader to a final concentration of 2 mM.

Excitation scans were performed on *P. patens* protonema tissue expressing *TKTP-roGFP2*: 100 μl of one-week-old liquid culture was transferred into a 96-well plate and either treated for 30 min with 10 mM DTT, 5 mM DPS or imaging buffer. Wells were excited at 390–490 nm using a monochromator while emission was collected at 535–16 nm. Intensities of excitation spectra were normalized to the intensity of the isosbestic point of roGFP2 at c. 425 nm.

2.8. CO₂ exchange measurements

CO₂ exchange measurements were performed with the GFS-3000 (Heinz Walz GmbH, Effeltrich, Germany). For each measurement, WT, $\Delta grxc5\#54$, and $\Delta grxc5\#249$ protonema cultures were cultivated in

parallel to a similar density in liquid medium. Three days after sub-culturing, 5 ml of each culture were applied onto a nylon membrane filter with a diameter of 35 mm, placed within a miniature Petri dish (\varnothing 42 mm). Any excess liquid was removed using a 1000 μl pipette tip. CO₂ uptake was recorded for 7.5 min in light (75 $\mu\text{mol photons m}^{-2}\text{s}^{-1}$), followed by 7.5 min in darkness. These measurements were performed consistently at a humidity level of 98 % and a temperature of 22 °C, with this cycle repeated three times per biological replicate to ensure reliability. To establish a baseline measurement, a nylon membrane filter wetted with KNOP-ME medium was used as a blank (zero point; ZP) before each measurement. The recorded ZP value was subtracted from each measurement point (MP). In Fig. 6, data from the last 2.5 min of the first dark cycle to the third dark cycle (dark-light-dark transition) from five biological replicates from different weeks were plotted.

2.9. SDS-PAGE and Western blotting

Protein extraction based on chloroform-methanol precipitation was performed according to [59,63] on frozen and pulverized plant material using the TissueLyser II (Qiagen). 100 μl lysis buffer (7.5 M urea, 2.5 M thiourea, 12.5 % (v/v) glycerol, 62.5 mM Tris-HCl pH 8, 0.1 % (v/v) Sigma plant protease inhibitor cocktail (P9599)) was added per 10 mg pulverized plant material. Additionally, protein thiol groups were blocked by a final concentration of freshly balanced 20 mM N-ethylmaleimide (NEM, Sigma 128-53-0) directly added to the lysis buffer. Protein pellets were dissolved in 50–100 μl protein resuspension buffer (50 mM Tris-HCl, 8 M urea, pH 7.5–8). SDS-PAGE samples were prepared by mixing the proteins sample with 1x non-reducing Laemmli buffer (2 % (w/v) SDS, 50 mM Tris-HCl pH 6.8, 0.002 % (w/v) bromophenol blue, 10 % (v/v) glycerol), and size-separated using 10 % Mini-PROTEAN® precast gels (Bio-Rad) (SDS-running buffer 25 mM Tris-HCl pH 8.3, 192 mM glycine, 0.1 % (w/v) SDS) according to the manufacturer's instructions, using 5 μl PageRuler™ Prestained Protein Ladder (ThermoFisher) as marker. Equal loading was confirmed by staining for >1 h in PageBlue™ protein staining solution (ThermoFisher).

Proteins were transferred to a PVDF membrane (Immobilon-P, Millipore Corporation, Billerica, MA, USA) via semi-dry Western blotting. The membrane containing the proteins was blocked in 5 % (w/v) milk powder dissolved in TBS-T buffer (20 mM Tris-HCl pH 7.6, 137 mM NaCl, and 0.1 % (v/v) Tween20) for 1 h at 25 °C or overnight at 4 °C before labelling with the primary antibody (α -GSH, ThermoFisher, MA1-7620, 1:1000 in 2.5 % (w/v) milk powder dissolved in TBS-T). Membranes were washed three times with TBS-T for 5 min and incubated for 1 h in the secondary antibody (Goat anti-Mouse, Agrisera, AS11 1772, 1:2500 in TBS). For immunodetection the Agrisera ECL kit (Super Bright, AS16 ECL-SN) was used according to the recommendations of the supplier. Western blots were imaged using the INTAS ECL ChemoStar imaging system (Intas).

3. Results

3.1. PpGRXC5 is a class I GRX with (de)glutathionylation activity

First, we determined PpGRXC5 (de)glutathionylation activity and kinetic parameters *in vitro*, by cloning and purifying PpGRXC5 (removing the N-terminal targeting sequence, starting with Ala120). We characterized K_m^{app} and $k_{\text{cat}}^{\text{app}}$ of PpGRXC5 using the hydroxyethyl disulfide (HED)-assay. PpGRXC5 was able to very efficiently catalyse the GSH-dependent reduction of S-glutathionylated β -mercaptoethanol [64] with catalytic efficiencies ($k_{\text{cat}}^{\text{app}}/K_m^{\text{app}}$) of $1.0 \times 10^5 \text{ M}^{-1}\text{s}^{-1}$ and $2.8 \times 10^4 \text{ M}^{-1}\text{s}^{-1}$ when HED and GSH were used a variable substrate, respectively (Fig. 2A). These catalytic efficiency constants are in a comparable order of magnitude with class I GRX7 from *S. cerevisiae*, *Plasmodium falciparum* [65] and class I GRXs from the green lineage, such as *Chlamydomonas reinhardtii* GRX1 [50], poplar PtGRXS12 [66,67] and AtGRXC5 [46].

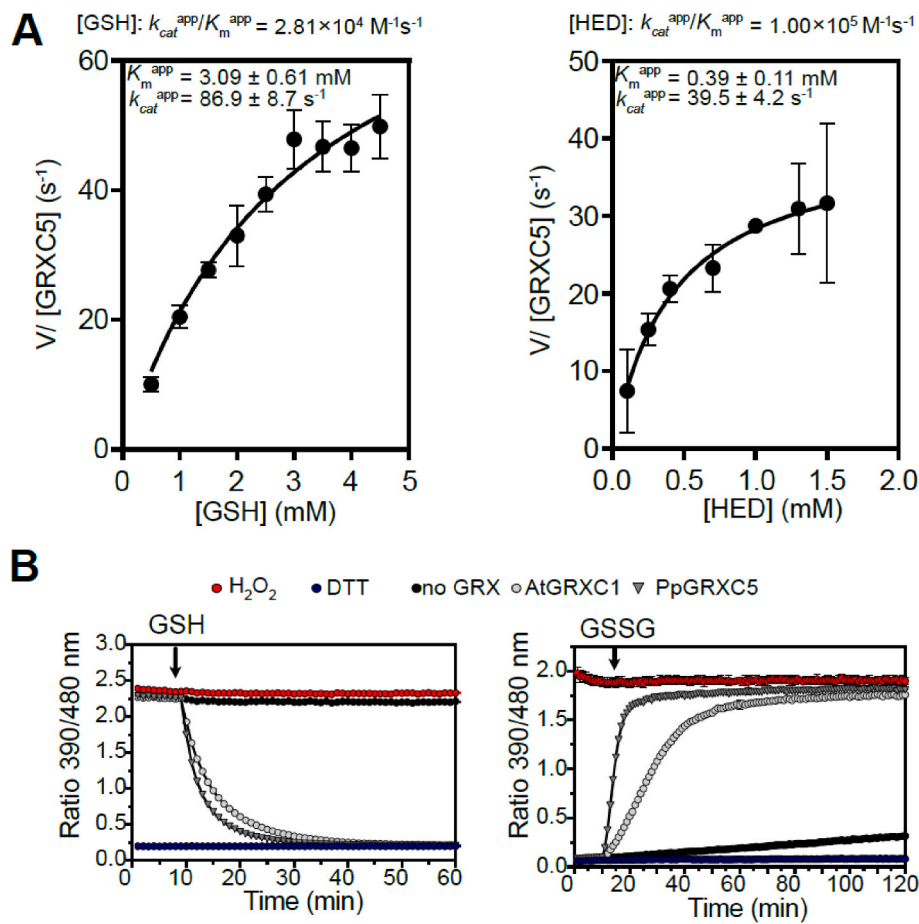


Fig. 2. Catalytic activity of PpGRXC5 *in vitro* (A) HED assays: PpGRXC5 [30 nM] was added to a cuvette containing GSH [0.5–4 mM], HED [0.3–1.5 mM], NADPH [200 μ M], GR [6 μ g/ml] in 100 mM Tris-HCl, 1 mM EDTA, pH 7.9. The decrease in absorbance at 340 nm was followed for 1 min (shown are means \pm SDs, $n = 4$). Varying concentration of GSH [0.5–4 mM] and a constant HED concentration of 0.7 mM was used to determine GSH-dependent kinetics (left panel). Varying concentrations of HED [0.3–1.5 mM] and a concentration of 1 mM GSH was used to determine HED-dependent kinetics (right panel). Apparent K_m (K_m^{app}) is depicted in mM, apparent k_{cat} (k_{cat}^{app}) in s^{-1} and the rate constant (k_{cat}^{app}/K_m^{app}) in $\text{M}^{-1}\text{s}^{-1}$. Non-linear regression was fitted using Prism 9 (GraphPad). (B) roGFP2 reduction assay (left panel): 1 μ M of PpGRXC5 or 1 μ M AtGRXC1 were incubated with 1 μ M of oxidized roGFP2 in 100 mM KPE, pH 7.4. Arrow indicates the time point of addition of 2 mM GSH; $n = 3 \pm$ SDs. roGFP2 oxidation assay (right panel): 1 μ M of PpGRXC5 or 1 μ M of AtGRXC1 were incubated with 1 μ M of pre-reduced roGFP2. Arrows indicate the time point of addition of 40 μ M GSSG. As oxidation and reduction controls (calibration), 1 μ M of roGFP2 was treated with 10 mM of DTT or 10 mM H₂O₂; $n = 3 \pm$ SDs.

As class I GRXs show oxidoreductase activity on disulfides that are formed and released via a *S*-glutathionylation intermediate [27,68], redox-sensitive GFP2 is a suitable target protein for *in vitro* assays, providing a direct fluorescent read-out for disulfide redox state [41–43, 69]. Hence, we tested PpGRXC5 oxidizing and reducing activity on recombinant roGFP2, in a direct comparison with the previously characterized AtGRXC1 [29] (Fig. 2B). In the *in vitro* roGFP2 reduction and oxidation assays PpGRXC5 was able to reduce and oxidise roGFP2 kinetically faster than AtGRXC1, confirming high activity in the reductive half-reaction and additionally showing high activity in the oxidative half-reaction of thiol-disulfide oxidoreductase function. Thus, PpGRXC5 is a typical class I GRX that shows efficient (de)glutathionylation as well as thiol-disulfide oxidoreductase activities.

3.2. The single stromal class I GRX PpGRXC5 is dispensable and not a main cause for the dwarfism in $\Delta gr1$ mutants

To generate null mutants of PpGRXC5 in *P. patens* we used homologous recombination (Fig. 3A). We confirmed several independent transgenic lines of which we used the null mutants $\Delta grxc5\#54$ and $\Delta grxc5\#249$ (Fig. S1) for further experimentation. Growth under standard conditions was comparable to the wildtype (WT) (Fig. 3B), which is in contrast to the previously characterised dwarfed *P. patens* glutathione

reductase knockout lines ($\Delta gr1$) that exhibit a less reducing stromal steady-state E_{GSH} [40]. We hypothesised that the defects observed in $\Delta gr1$ might be dependent on PpGRXC5 function. On the one hand, PpGRXC5 could contribute to plastid GSSG generation by using GSH as electron donor. On the other hand, PpGRXC5 could mediate disadvantageous *S*-glutathionylation in response to an oxidative shift in the local glutathione pool (Fig. 1). To this end, we generated $\Delta gr1/\Delta grxc5$ double knock-outs by transforming the PpGR1 knock-out construct [40] into protoplasts of $\Delta grxc5\#54$ and confirmed the correct integration and absence of transcript for *GR1* (Fig. S1). Lack of GRXC5 did not rescue the $\Delta gr1$ phenotype, as $\Delta gr1/\Delta grxc5$ mutant lines were dwarfed (Fig. 3B). Quantification of growth revealed a trend for increased fresh weight of $\Delta gr1/\Delta grxc5$ compared to $\Delta gr1$, that was not statistically significant (Fig. S2). In addition, $\Delta gr1/\Delta grxc5$ showed the same sensitivity to H₂O₂-induced oxidative stress as $\Delta gr1$ (Fig. 3C). Thus, GSSG generation by PpGRXC5 is not contributing to the major defects observed in $\Delta gr1$ lines.

To further test for altered stress resilience or growth defects in $\Delta grxc5$ lines, we exposed plants to low light, fluctuating low light/high light and heat, but did not identify any morphological differences to WT (Fig. S3). To test for differences in photosynthetic light reactions, we determined light-induction and relaxation kinetics, calculating non-photochemical quenching (NPQ) under control conditions and after

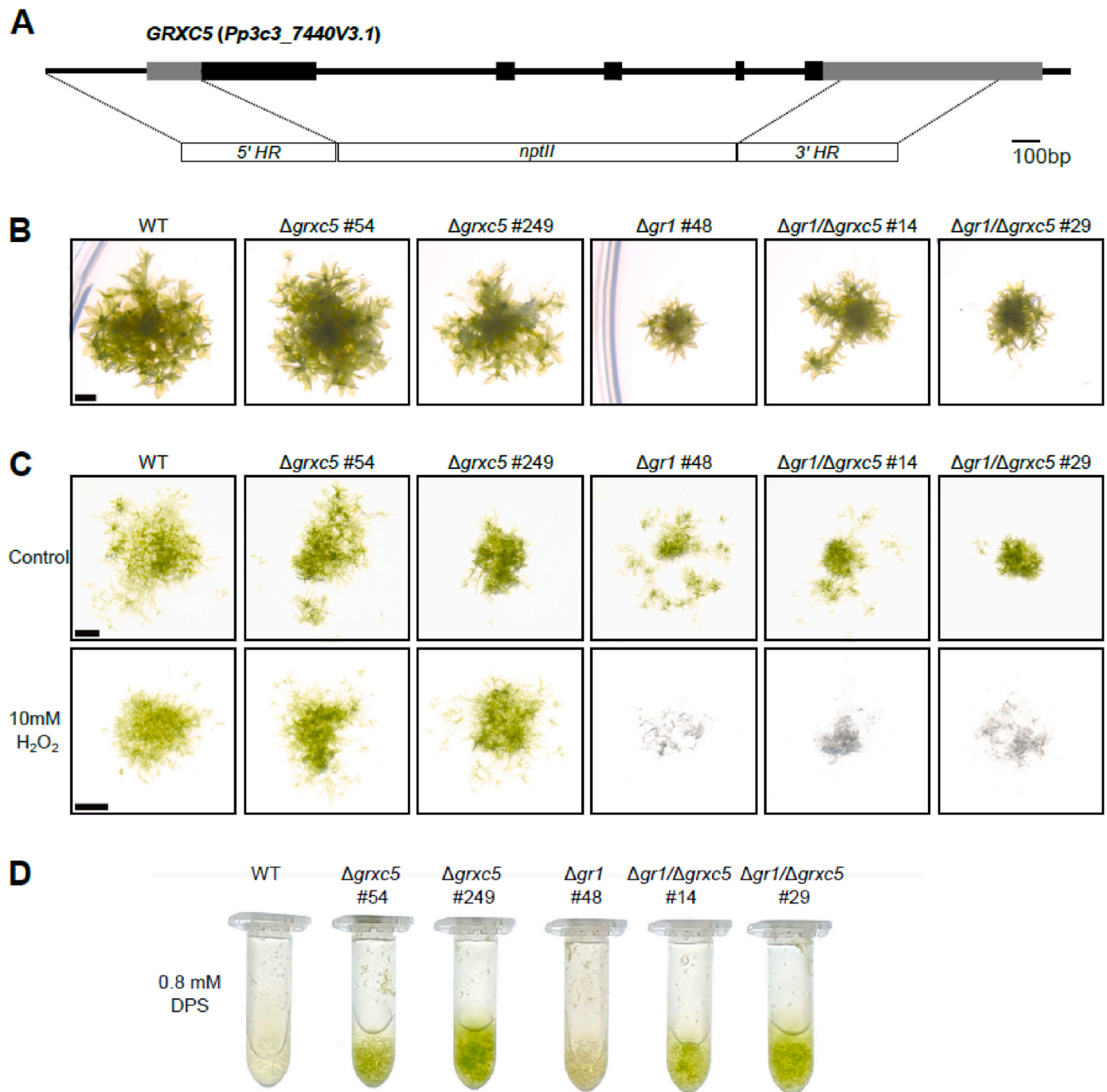


Fig. 3. Phenotype of $\Delta grx5$, $\Delta gr1$ and $\Delta gr1/\Delta grx5$ plants (A) Schematic overview of the PpGRXC5 gene structure and knock-out construct; exons = boxes; UTRs (untranslated regions) light grey, coding sequence black; HR, homologous regions; *nptII*, neomycin phosphotransferase resistance cassette. (B) *P. patens* grown on KNOP-ME pH 5.8 agar plates in 100 $\mu\text{mol photons m}^{-2}\text{s}^{-1}$ (16 h light, 8 h dark) for four weeks, scale bar = 1 mm. Row represents colonies grown on the same plate. (C) Protonema culture spotting assay on KNOP-ME plates after incubating with 10 mM of H₂O₂ for 15 min as oxidative challenge. A 20 μl aliquot of protonema culture was placed on a KNOP-ME agar plate and grown under 60 $\mu\text{mol photons m}^{-2}\text{s}^{-1}$ (16 h light, 8 h dark) for 7 days. Control cultures were treated equally except for addition of H₂O₂. Images were taken after 7 days of recovery. Scale bar: 1 mm. (D) Three-day-old protonema culture was further grown in presence of 0.8 mM DPS (2,2'-dipyridyl disulfide) for 4 d (100 $\mu\text{mol photons m}^{-2}\text{s}^{-1}$ (16 h light, 8 h dark), shaking).

exposure to high light (450 $\mu\text{mol photons m}^{-2}\text{s}^{-1}$). $\Delta gr1$ plants showed increased non-photochemical quenching (NPQ) combined with retarded relaxation kinetics consistent with a previous report [40], while $\Delta grx5$ lines did not show any significantly different response in NPQ induction or relaxation (Fig. S4). Our results confirm that neither the growth defect nor the sensitivity to high light of $\Delta gr1$ plants is detectable in $\Delta grx5$ plants, indicating that the negative effects of the less negative E_{GSH} in $\Delta gr1$ plants are not mediated via GRXC5. Instead, $\Delta grx5$ plants

showed WT-like growth in all long-term stress assays.

As *S. cerevisiae grx1/grx2* mutants showed decreased sensitivity to diamide [70], we compared $\Delta grx5$ mutant lines to WT, $\Delta gr1$ and $\Delta gr1/\Delta grx5$ lines after exposing them to a thiol-specific oxidant (Fig. 3D). We found an increased resistance towards DPS (2,2'-dipyridyl disulfide) in all lines lacking $\Delta grx5$. Thus, in severe thiol-oxidizing conditions *in vivo* PpGRXC5 activity is disadvantageous, potentially catalysing *S*-glutathionylation on physiologically relevant specific

targets.

3.3. Lack of class I GRX leads to distinct roGFP2 oxidation state and changed reduction kinetics after oxidative challenge in the stroma

As we did not identify phenotypical deviations of $\Delta grx5$ lines from WT macroscopically under physiologically relevant conditions, we sought to investigate stromal redox dynamics *in vivo* by introducing a genetically encoded biosensor. Redox-sensitive GFP2 (roGFP2) specifically equilibrates with the steady-state E_{GSH} of the local subcellular compartment [41,43]. As this equilibration is catalysed by class I GRX, human GRX1 (hGrx1) fused to roGFP2 (Grx1-roGFP2) is the standard probe used, to guarantee independence from local endogenous GRX activities [42]. Since it was our aim to measure the endogenous GRX activity we exploited the requirement of GRX-mediated equilibration and targeted roGFP2 without fused hGRX1 to the plastid stroma of WT and $\Delta grx5\#54$ genetic backgrounds. We generated a construct for

expression of roGFP2 fused to the transketolase targeting peptide (TKTP) [43,56]), constitutively driven by the PpActin5 promoter, targeting roGFP2 to the plastid stroma. Exclusive targeting of roGFP2 to plastids in stable transgenic lines was confirmed microscopically (Fig. S5) and sensor lines for each background were characterised and selected for further analyses (TKTP-roGFP2 in $\Delta grx5\#54$ lines #17 and #21; TKTP-roGFP2 in WT #20).

Sensor responsiveness to oxidation/reduction *in vivo* was confirmed via addition of either 10 mM DTT (reductant) or 5 mM DPS (2,2'-dipyridyl disulfide, thiol-specific oxidant) to moss protonema. Using a fluorescence plate reader, excitation spectra for roGFP2 fluorescence were recorded (Fig. 4A), revealing a comparable dynamic range (between 2.0 and 2.2 (405/488)) of the sensor response in WT and $\Delta grx5$ background. In comparison to TKTP-roGFP2 WT#20, the physiological (untreated, Phys.) spectra of $\Delta grx5$ sensor lines revealed lower excitation above the isosbestic point (c. 425 nm) and higher excitation below 425 nm, showing increased oxidation of roGFP2 of c. 20 % (calculated

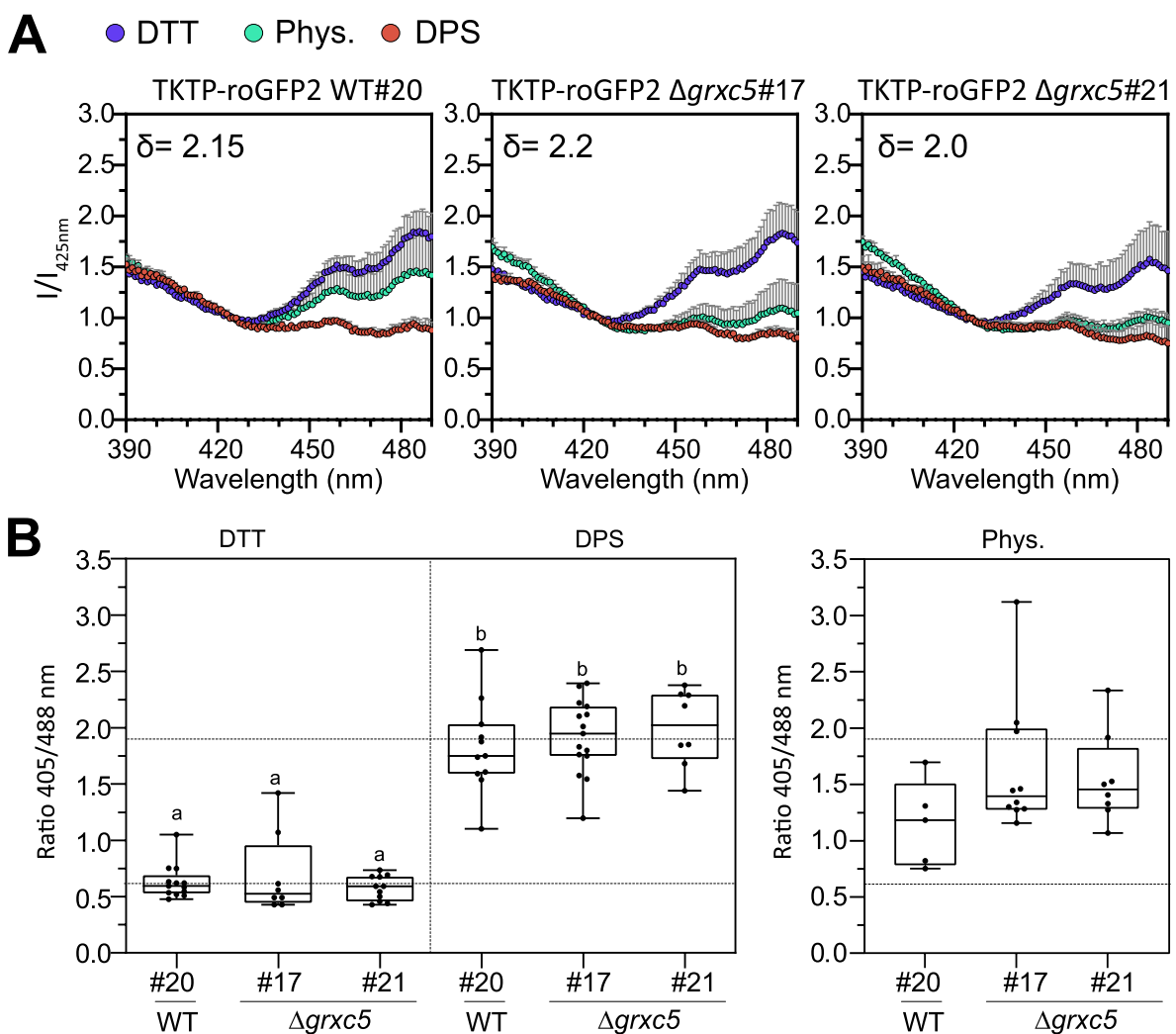


Fig. 4. Redox state of stroma-targeted roGFP2 in WT and $\Delta grx5$ (A) *In vivo* excitation spectra: protonema cultures of *P. patens* were not treated (Phys.) or treated for 30 min with 10 mM DTT or 5 mM DPS. Fluorescence was excited from 390 to 490 nm while emission was collected at 535–16 nm in a plate reader-based setup. Intensities were normalized to the intensity of the isosbestic point of roGFP2 (425 nm); $n = 3$, mean + SD. Delta depicts the dynamic range (405/488 nm) for each line. (B) Left panel: Image-based sensor calibration of TKTP-roGFP2 in *P. patens* with 10 mM DTT or 5 mM DPS incubated for at least 20 min before imaging with the CLSM (ex. 405, 488 nm; em. 508–535 nm); $n > 7$, box blots: line = median and whiskers = min/max values; two-way ANOVA and Tukey's multiple comparison test was conducted ($p < 0.0001$), different lowercase letters indicate significant difference, dynamic range c. 3.2. Right panel: image-based analysis of steady state sensor ratio (405/488 nm) under physiological conditions: *P. patens* protonema/gametophore culture was pre-incubated in the dark for 30 min before imaging with the CLSM (ex. 405, 488 nm; em. 508–535 nm); $n = 5$ –10 pictures, box blots: line = median and whiskers = min/max values, one-way ANOVA and Tukey's HSD test (ratio genetic background, $p = 0,08$); horizontal lines: 0 % and 100 % oxidation based on mean DTT and mean DPS values, according to sensor calibration, see left panel.

for 405/488 nm). We additionally quantified this oxidation by ratio-metric analysis of confocal images of the respective lines and found an increase in median 405/488 ratio of 1.64 ± 0.59 in $\Delta grxc5\#17$, 1.54 ± 0.40 in $\Delta grxc5\#21$ compared to 1.15 ± 0.38 in WT#20 (Fig. 4B). Taking into account sensor calibration (i.e., ratio values for complete reduction and oxidation *in vivo*), these values support a by c. 20 % higher degree of oxidation (OxD) on stromal roGFP2, compared to WT, in untreated cells.

As higher OxD values for roGFP2 are interpreted as a less negative stromal E_{GSH} , at least in the presence of GRX activity, we additionally quantified total GSH levels by HPLC from five biological replicate samples of protonema and found a trend for an increase in total glutathione in $\Delta grxc5\#54$ ($p = 0.15$) and a significant increase in total glutathione in $\Delta grxc5\#249$ ($p = 0.0006$), compared to WT (one-way ANOVA, Tukey's multiple comparison) (Fig. S6). These analyses suggest that loss of PpGRXC5 causes a higher steady state OxD of roGFP2 in the stroma, as well as a trend to increased GSH levels.

As long-time exposure to various stresses did not reveal any defects in $\Delta grxc5$ lines, we simulated a pulse of oxidative stress to generate a temporary oxidation and compared the subsequent recovery. We exposed moss protonema to 10 mM H_2O_2 , which causes complete oxidation of roGFP2. After removal of H_2O_2 , we monitored the recovery kinetics of roGFP2 reduction state. While the WT background showed a fast recovery almost immediately after removal of H_2O_2 , $\Delta grxc5$ null mutants showed slower, approximately linear recovery of roGFP2 redox state (Fig. 5A). Using lower H_2O_2 concentrations in a 1–5 mM range, fast recovery was already observable during the presence of exogenously added oxidant in the WT background while $\Delta grxc5$ null mutants consistently showed slower, approximately linear recovery from oxidative stress (Fig. S7). To additionally monitor oxidation kinetics of the dithiol on roGFP2, we pre-reduced moss protonema and subsequently used injection of H_2O_2 combined with 1.5 s measuring intervals. We found that oxidation of roGFP2 in $\Delta grxc5$ stroma proceeded equally

fast or slightly faster (Fig. 5B). Thus, disulfide formation in response to severe oxidative stress is fast in $\Delta grxc5$ null mutants while stromal GSH-dependent disulfide reduction is slow and almost linear.

3.4. Linking S-glutathionylation levels to oxidative challenge and GRX activities

Using roGFP2 enabled us to observe disulfide formation and reduction kinetics in the absence of a class I GRX under different environmental conditions. However, disulfides would only be formed in response to S-glutathionylation if a second cysteine is present in a suitable distance to reduce the mixed disulfide, forming an intramolecular disulfide and concomitant release of GSH (Fig. 1). While this is the case for roGFP2, many *in vivo* targets of class I GRXs may remain in a S-glutathionylated state [25,71]. Hence, we investigated if total protein S-glutathionylation levels are altered in $\Delta grxc5$ null mutants, using Western blotting with an anti-GSH antibody (Fig. 6). As a control, we incubated *in vitro* purified roGFP2 mutant lacking the resolving Cys204 (roGFP2C204S) [29] with 10 mM H_2O_2 in the presence of 2 mM GSH, inducing S-glutathionylation. Protein extracts from non-stressed and stressed WT and $\Delta grxc5$ plants both showed equally increased signal after immunodetection of protein-bound GSH, starting from a similar level. Increase of protein-bound GSH was consistent and independent of presence of GRXC5 after oxidative challenge (Fig. S8).

3.5. Stromal GSH-dependent redox kinetics are altered in dark/light/dark transitions, without an effect on carbon fixation

As stromal Grx1-roGFP2 showed previously unknown light/dark transition-dependent E_{GSH} dynamics in WT [40], we next assessed stromal roGFP2 redox dynamics in $\Delta grxc5$ null mutants using both a plate reader-based setup (Fig. 7A) and a confocal microscopy-based

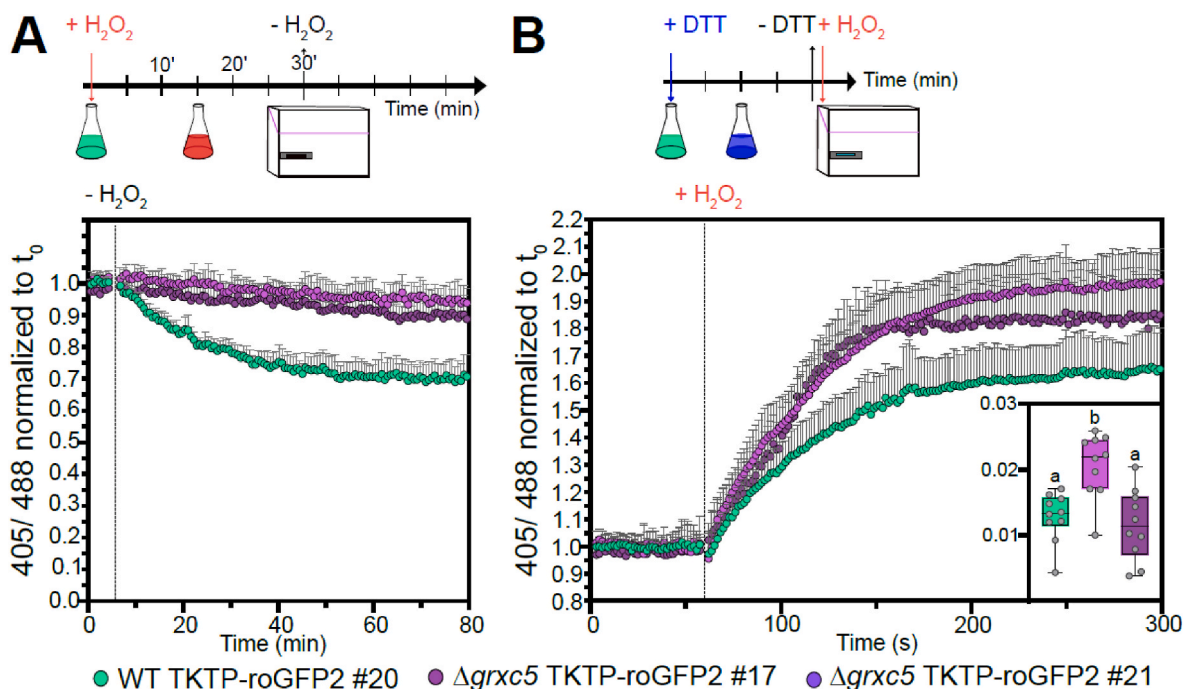


Fig. 5. *In vivo* kinetics of stromal roGFP2 in response to oxidative challenge (A) Protonema culture expressing *TKTP-roGFP2* was treated with 10 mM H_2O_2 for 30 min and H_2O_2 subsequently removed and exchanged with imaging buffer to monitor recovery from oxidative challenge (red flask). 405/488 nm ratio of $n = 6$ biological replicates was normalized to t_0 , graph depicts mean + SD. A two-way ANOVA with Tukey's multiple comparison test was conducted for each time point revealing significant differences in roGFP2 kinetics between WT and both $\Delta grxc5\#17$ and $\Delta grxc5\#21$ starting from 11 min after peroxide removal ($p < 0.001$, $n = 6$). (B) *In vivo* oxidation rates after injection of H_2O_2 (final concentration = 2 mM) and monitoring of 405/488 nm ratio every 1.55 s. Protonema culture expressing *TKTP-roGFP2* was pre-reduced using 10 mM DTT (blue flask). Shown are the mean + SD, $n = 10$, normalized to t_0 . Slope (inset, $\Delta R/\Delta t$) was calculated for the first 10 s after injection (eight data points). Box plot whiskers depict min and max values with the horizontal line indicating the median. One-way ANOVA with Tukey's multiple comparison test was conducted to test for significant difference ($p < 0.027$).

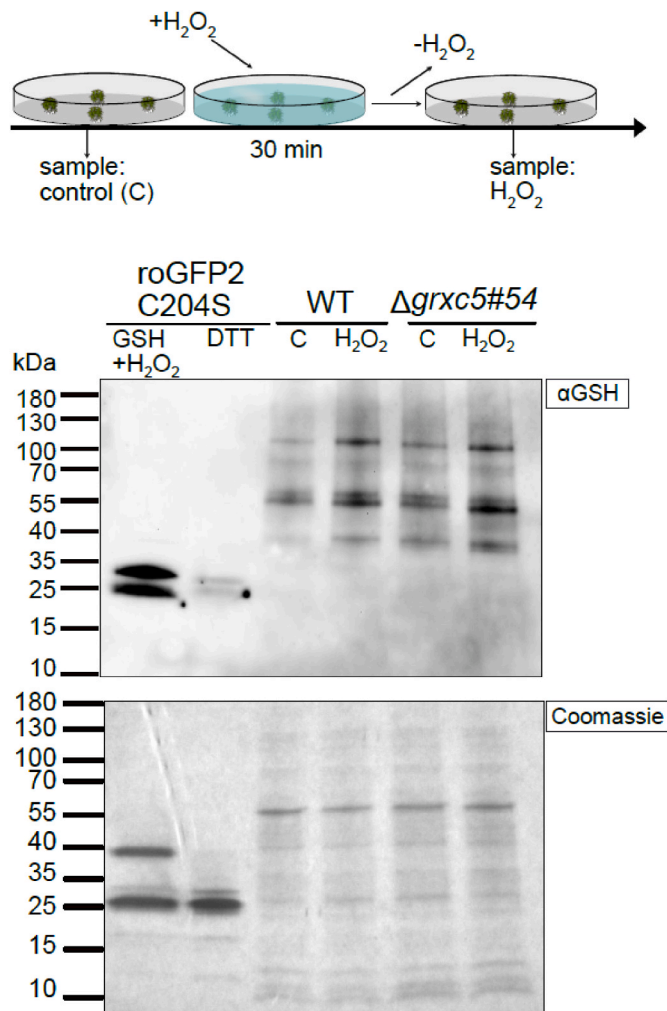


Fig. 6. Total protein-bound glutathione after oxidative challenge **(A)** Schematic overview of the experimental set-up and sampling. **(B)** Immunoblot using α -GSH (ThermoFisher). Total protein extracts from *P. patens* WT and $\Delta grxc5\#54$ gametophore tissue either non-treated ('C') or treated with 10 mM H₂O₂ for 30 min ('H₂O₂') (see panel A); cysteine oxidation was blocked with 20 mM NEM (*N*-ethyl maleimide) in the lysis buffer. As loading control, 10 μ g total protein was loaded onto a 4–20 % gradient non-reducing SDS-PAGE (lower panel). As control for antibody specificity, purified roGFP2C204S (10 μ M) was treated with 10 mM H₂O₂ in the presence of 2 mM of GSH for 30 min (positive control, glutathionylated roGFP2C204S) or treated with 10 mM DTT (negative control, no glutathionylated roGFP2C204S), and 12 μ l loaded per lane.

setup [40] (Fig. 7B). We found that light/dark transition-dependent dynamics of stromal roGFP2 oxidation state were also observable using roGFP2 without fused Grx1 in WT background: a sudden light to dark transition leads to rapid sensor oxidation, followed by a recovery phase. In contrast, light/dark dependent roGFP2 redox changes were completely absent in $\Delta grxc5$ null mutants. Responsiveness of the roGFP2 probe was confirmed after light/dark treatment by calibration (Fig. 7A), demonstrating that roGFP2 redox state in $\Delta grxc5$ was well inside dynamic range of roGFP2. As a complementary approach, we used a CLSM-based setup where we were also able to follow roGFP2 redox state in the light and confirmed absence of dark/light/dark transition-dependent roGFP2 redox dynamics in $\Delta grxc5$ (Fig. 7B).

As our results suggest potential differences in glutathione-dependent redox dynamics in the chloroplast stroma, we assessed cross-talk to the TRX system by quantifying CO₂ release and assimilation from protinema in a dark/light/dark transition (Fig. 7C). Our analysis did not find any significant differences in either CO₂ release in the dark, nor in CO₂

uptake in the light, suggesting overall unaltered redox-regulation of the CBB cycle enzymes in $\Delta grxc5$ lines, compared to WT. Thus, fast responses of the roGFP2 redox state to light/dark dependent E_{GSH} dynamics are absent in $\Delta grxc5$ plants, while regulation of carbon fixation was unaltered under the tested conditions.

4. Discussion

4.1. Glutathione as an electron donor in the plastid stroma

The redox state of protein thiols depends on their reaction kinetics with different small molecules or protein reductants and oxidants at defined concentrations. In many cases, the respective reactions involve additional thiols in a suitable distance for disulfide formation and/or protein-protein interactions. Different thiol/oxidized thiol redox couples can be in thermodynamic equilibrium after incubation in the range of minutes to hours, whereas enzymatically catalysed equilibration takes place in the range of seconds to minutes. GRX-catalysed redox equilibration depends on GSH as electron donor. We determined the enzyme kinetics of PpGRXC5 (YCPYC active site) *in vitro* and found high deglutathionylation activity (HED assays) as well as thiol-disulfide oxidoreductase activity (roGFP2 *in vitro* assays). The apparent second-order rate constant(s) ($k_{\text{cat}}^{\text{app}}/K_{\text{m}}^{\text{app}}$) for PpGRXC5-catalysed reactions (HED assay) was similar to AtGRXC1 (YCGYC active site) [72] or AtGRXC5 (WCSYC active site) [46], showing that GRXC5 is an evolutionary conserved redoxin [25] with a typical class I GRX functionality as GSH-dependent (de)glutathionylation and thiol/disulfide oxidoreductase activity.

Disulfides can be characterized by their midpoint potential, *i.e.*, the redox potential at which 50 % of the molecules are reduced and 50 % oxidized. The disulfide formed by the genetically encoded biosensor roGFP2 is well-characterised, with a consensus midpoint potential of -280 mV (pH 7), and enzymatically catalysed by GRX in dependence on E_{GSH} ([41,42,73]; reviewed in Meyer and Dick [69]; Schwarzländer et al. [38]; Müller-Schüssele et al. [74]). Here we targeted roGFP2 to the plastid stroma of *P. patens*, without a fused GRX, to track local GSH-coupled redox dynamics. In WT plants, the roGFP2 redox state indicated a steady-state stromal E_{GSH} of c. -312 mV (pH 8), consistent with the -311 mV (pH 8) measured using Grx1-roGFP2 in WT background of *P. patens* plastid stroma [40]. A similar physiological steady-state stromal E_{GSH} in the dark-adapted state of WT using either roGFP2 or Grx1-roGFP2 confirms similar functionality of roGFP2 in WT stroma, without fused human Grx1. Compared to WT, we detected an increased 405/488 nm ratio and corresponding increased degree of oxidation for roGFP2 (OxD_{roGFP2}) of c. 20 % in the stroma of $\Delta grxc5$ lines. In addition, we found a trend for increased total GSH content, which would according to the Nernst equation suggest more negative E_{GSH} , although HPLC measurements do not allow for subcellular resolution. A shift of roGFP2 thiol/disulfide redox state to more oxidized values usually reveals an oxidative shift in E_{GSH} , as roGFP2 specificity for the glutathione/GRX system was tested *in vitro* and *in vivo* [29,41,65,75]. Particularly, inefficient reduction of GSSG caused by absence of GR leads to an increase of OxD_{roGFP2} in the same subcellular compartment [39,40,45]. In $\Delta gr1$ lines, a shift of c. 44 % in OxD_{roGFP2} was measured using stroma-targeted Grx1-roGFP2 which reports an oxidative stromal E_{GSH} shift of c. 33 mV [40]. In theory, the measured shift in roGFP2 redox status in the $\Delta grxc5$ lines may indicate either altered E_{GSH} , *i.e.*, local decrease in GSH and/or local increased GSSG concentration, or inefficient equilibration between E_{GSH} and roGFP2 (or a combination of both). The following argument supports an oxidative shift in OxD_{roGFP2} in the $\Delta grxc5$ stroma independent of a change in local E_{GSH} : (1) GR is still present in the stroma of $\Delta grxc5$, safeguarding the highly reducing stromal E_{GSH} . (2) *In vivo* stromal roGFP2 reduction rates after oxidative challenge (Fig. 5A) are similar (*i.e.*, in the range of minutes to hours) to thermodynamically driven *in vitro* reduction rates based on highly negative E_{GSH} , but lacking addition of GRX (Fig. 2B [41]). Thus, without

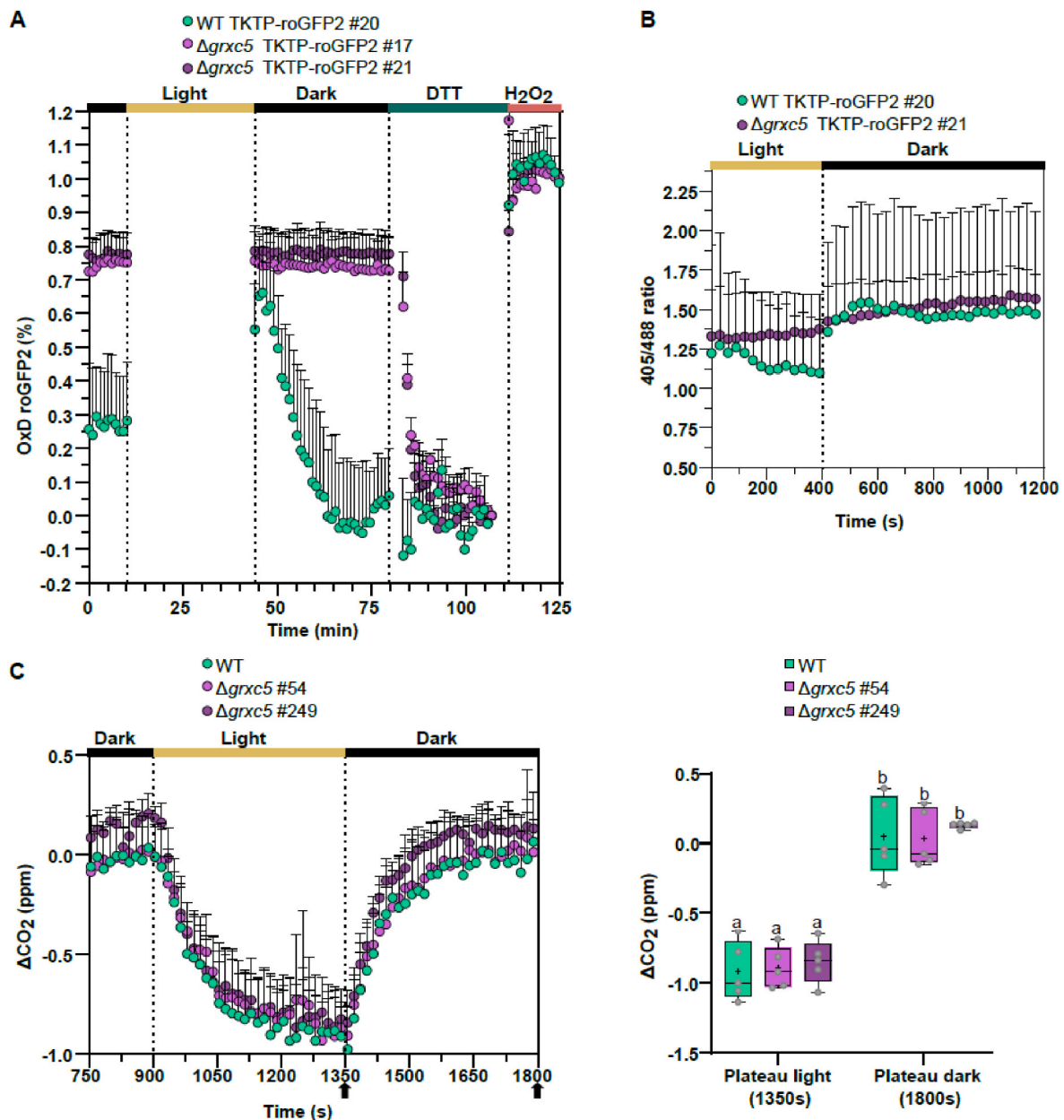


Fig. 7. Light-dependent roGFP2 dynamics and CO₂ assimilation during dark-light-dark transitions in protonema culture of $\Delta grxc5$ and WT (A) Reduction/oxidation dynamics in dark/light/dark transitions. In a 96-well plate with 200 μ l of protonema culture from *P. patens*, initial fluorescence was measured after 30 min dark incubation using a plate reader-based setup. Subsequently, the plate was illuminated for 30 min to an intensity of ~ 200 μ mol photons $m^{-2}s^{-1}$ using external LED illumination. After dark/light/dark transition, each well was calibrated by first replacing the buffer with 10 mM DTT and then 10 mM H₂O₂. OxD = degree of oxidation, shown are the mean (+SD) of $n = 3$. (B) Image-based analysis of oxidation/reduction dynamics of TKTP-roGFP2 in *P. patens* gametophores and protonema tissue grown in liquid culture. CLSM time series of dark-adapted samples: 1 min in the dark, illumination by external light source for 5 min (100 μ mol photons $m^{-2}s^{-1}$), followed by dark incubation. Images were taken every 30 s for 20 min; shown is the mean + SD of $n = 7-8$. (C) Left panel: changes in CO₂ partial pressure during dark/light/dark transitions in protonema culture of $\Delta grxc5$ lines and WT using a 7.5 min light and 7.5 min dark cycle (98 % humidity, 500 ppm CO₂, 22 °C, and 75 μ mol photons $m^{-2}s^{-1}$). The absolute changes in CO₂ levels were measured after zero-point (ZP) subtraction (nylon membrane filter wetted with KNOP-ME as ZP). Right panel: Changes in CO₂ partial pressure after reaching plateau values during the light and dark phases, respectively (indicated by arrows in left panel). One-way ANOVA and Tukey's multiple comparison to assess significant differences between $\Delta grxc5$ lines and WT at the end of the light cycle (1350 s) and the end of the dark cycle (1800 s): $p = 0.99$. Boxes display the 25–75 percentiles, with the minimum and maximum values indicated by the whiskers, and the median marked by the horizontal line ($n = 5$).

class I GRX present, a shifted OxD_{roGFP2} likely originates from a decreased glutathione-dependent reduction rate of the roGFP2 disulfide, never reaching thermodynamic equilibrium with E_{GSH} . Instead the interaction with other redox couples becomes apparent in the form of the oxidation (*i.e.*, unchanged oxidation rates), resulting in an OxD_{roGFP2} steady state further away from thermodynamic equilibrium with glutathione as electron donor (schematic model Fig. 8). After oxidative

challenge, lack of GRXC5 activity causes slow recovery rates from higher thiol oxidation levels (Fig. 8). Thus, $\Delta grxc5$ and $\Delta gr1$ mutants both show altered OxD_{roGFP2} *in vivo*, but through different mechanisms, *i.e.*, lacking reduction of GSSG vs. kinetic uncoupling between E_{GSH} and thiol/disulfide redox state. Our data show that fast enzymatically catalysed equilibration of roGFP2 redox state with the highly reduced glutathione pool is not complemented by other redox systems present in the stroma

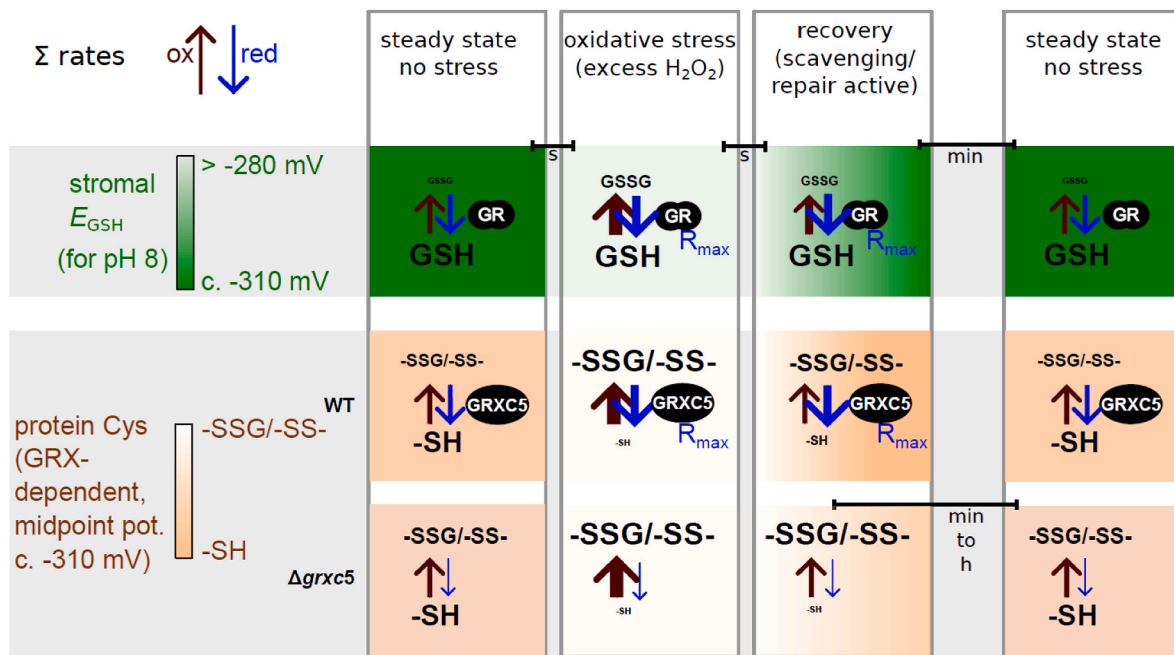


Fig. 8. Schematic overview: Model of observed dynamic redox states as a consequence of changing oxidation and reduction rates. Simplified scheme of steady states of the GSH/GSSG redox couple and resulting E_{GSH} , as well as the protein thiol/disulfide and thiol/glutathionylated redox couples before, during and after an oxidative challenge, as investigated in this work using roGFP2. Redox potentials are given for pH 8 (midpoint potential of roGFP2 at pH 8 is -310 mV). Colour scales exemplify relative changes between reduced and oxidized forms. Bars indicate approximate durations of transitions. Arrow thickness indicates sum of oxidation rates (i.e. all direct oxidation (slow) and enzymatically catalysed oxidation (fast)) and sum of reduction rates that would result in the observed profile of redox dynamics. Lack of GRXC5 leads to more oxidized steady state for target cysteines, as well as slow recovery rates. Enzymes are depicted as black ovals. R_{max} = maximal reachable reduction rate with current enzyme copy number.

and confirm GRXC5 as the sole stroma-targeted class I GRX in *P. patens*.

Moreover, by generating $\Delta\text{grxc5}/\Delta\text{gr1}$ double mutant lines, we found that GRXC5 function is not a main cause for the stress-sensitive and dwarfed Δgr1 phenotype. This excludes GRXC5 as main GSSG-producing enzyme in the stroma. Glutathione can serve as electron donor for other stromal enzymes involved in ROS-induced damage repair or ROS scavenging, such as GST iota/lambda (glutathione *S*-transferases) and DHAR (dehydroascorbate reductase) (reviewed in Müller-Schüssele et al. [25]). Thus, enzymatic contributions to localised GSSG generation (see GSH oxidation rates in Fig. 8) merit further investigation.

4.2. Is class I GRX function relevant in the chloroplast stroma?

TRX and GRX functions are partially redundant in *E. coli*, mostly related to their function as alternative electron donors to ribonucleotide reductase, powering cell growth [26]. In *S. cerevisiae*, $\Delta\text{grx1}/\Delta\text{grx2}$ null mutants grow normally but show increased sensitivity to oxidative challenge as well as decreased sensitivity to diamide [70,76]. Lethality only occurred when concomitantly knocking-out all cytosolic TRX isoforms [36], whereas one cytosolic monothiol GRX was able and sufficient to compensate for loss of all TRX and GRX [77]. Notably, Δgrxc5 lines did not show a decreased resistance to H_2O_2 -induced oxidative stress (as observed in Δgr1), but they were more resistant to DPS-induced thiol oxidation stress compared to WT and Δgr1 (Fig. 3). A possible explanation might be that PpGRXC5 catalyses *S*-glutathionylation of its endogenous target proteins in response to GSH oxidation by DPS, while *S*-glutathionylation would be slow or absent on many cysteines in response to H_2O_2 via a sulfenic acid intermediate [20]. During land plant evolution, a second isoform of plastid-targeted class I GRX lacking the second active site Cys, GRXS12, evolved within the same clade [25]. Poplar GRXS12 was characterized as functional monothiol class I GRX [66,67], but the biological relevance of either class I GRX plastid isoform remains so far unclear.

While E_{GSH} is usually robust, except under extreme abiotic stress

conditions challenging GR capacity [49,62,78] (Fig. 8), recent results have shown that stromal E_{GSH} is dynamic in response to physiological light/dark transitions [40,44]. We found that in Δgrxc5 stroma, these light-dependent E_{GSH} dynamics are not transferred anymore to glutathione-dependent disulfides, such as in roGFP2 (Fig. 7A), raising the question which endogenous target disulfides may respond differently (Fig. 8). As an obvious target for interference between the TRX and GSH/GRX system in the stroma, we tested CO_2 release and uptake in WT compared to Δgrxc5 lines and found no significant differences under the tested conditions (Fig. 7B). In accordance with the normal plant growth observed in Δgrxc5 lines, this result indicates that TRX-dependent redox regulation of the CBB cycle (TRX-*m* and TRX-*f* isoforms) is not affected. This confirms limited cross-talk between the TRX and class I GRX in the plastid stroma.

The remaining question is why GSH/GRX and TRX-dependent redox cascades can remain largely separated in the same subcellular compartment. One possible explanation is substrate specificity, e.g. mediated by electrostatic complementarity between redoxins and their target proteins [79]. As at least one stromal class I GRX isoform (GRXC5 or GRXS12) is evolutionarily strictly conserved, an important function is likely, but may not consist in backing-up TRX-dependent redox cascades. In accordance, plastid-localised PRXIII that is efficiently reduced via class I GRX, does not function as TRX oxidase like other PRX [80].

4.3. *S*-glutathionylation: A needle in the haystack or important PTM?

A remaining important question is for which plastid processes fast GRX-mediated reduction kinetics of either protein *S*-glutathionylation or GSH-dependent protein disulfides would matter. By exogenously challenging plants with H_2O_2 , we found that kinetically fast roGFP2 reduction was absent in the stroma. This leads to prolonged disulfide persistence in a time frame of at least 30 min after such an oxidative challenge, as well as to an altered steady state OxD. Thermodynamic equilibration of purified proteins with E_{GSH} can take hours [41]. In

contrast, initial oxidation kinetics for stromal roGFP2 after an imposed oxidative challenge by addition of H₂O₂ were not slower in Δ grxc5 lines, compared to WT (Fig. 5B). Disulfides can be directly induced by H₂O₂, with the rate constant being dependent on the pK_a of the more reactive cysteine [81]. In this case, the thiolate anion reacts with H₂O₂, forming a sulfenic acid (-SOH) and water. This sulfenic acid can react with a nearby thiol, forming a disulfide (and water). In the presence of GSH, this reaction sequence can lead to GRX-independent S-glutathionylation. Using an anti-GSH antibody on stressed and control samples of WT and Δ grxc5 lines we found increased total S-glutathionylation after oxidative challenge. Lack of GRXC5 did not interfere with the level of glutathionylated proteins after H₂O₂-induced oxidative stress treatment (Fig. 6, Fig. S8), indicating a minor contribution of GRXC5-mediated S-glutathionylation under the tested conditions. Our results support the hypothesis that the most likely scenario for protein S-glutathionylation (and S-glutathionylation-dependent disulfide formation) *in vivo* involves activated thiol derivatives such as sulfenic acids, most efficiently formed on cysteine residues that are in a deprotonated state (*i.e.*, thiolates) at physiological pH [71].

Previous studies have revealed around 150 stromal proteins as potential S-glutathionylation targets, using different experimental approaches (reviewed in Zaffagnini et al. [81] and Müller-Schüssele et al. [25]). However, it is still unclear under which physiological conditions which fraction of principally susceptible cysteine residues really is S-glutathionylated *in vivo*, including consequences to activity, stability or localization of the affected protein molecules. If S-glutathionylation only occurs for a minor fraction of proteins or a minor fraction of protein molecules of one protein isoform, effects on metabolic fluxes would be unlikely, as there are still many non-glutathionylated protein molecules present in the entire population. However, protein cysteines with stable thiolate anions are interesting candidates to sense H₂O₂ or oxidative shifts of the glutathione pool in signalling processes, with reduction rates mediated via class I GRX. In this regard, cytosolic GAPDH provides an interesting example. This enzyme contains a reactive cysteine which is essential for catalysis and is a major target of H₂O₂-dependent oxidation [82,83]. The subsequent reaction of GSH with the sulfenylated catalytic cysteine induces S-glutathionylation and protects the enzyme from irreversible oxidation. However, the persistence of the glutathionylated state, which causes an unavoidable loss of function, has a drastic and irreversible effect on structural stability inducing protein misfolding and aggregation [84].

In order to understand the biological relevance of protein S-glutathionylation as PTM in the chloroplast stroma, identification of *in vivo* targets of GRXC5 (and/or GRXS12 in angiosperms) is necessary. This task will require fitting methodological tools for high-throughput protein redox state analysis in combination with suitable mutants and time frames. Life imaging with genetically encoded redox sensors can meet the challenge to follow oxidation and reduction rates *in vivo*, and to effectively dose stress treatments.

Based on our results, we conclude that stromal class I GRXs are necessary to quickly release S-glutathionylation or disulfides formed via an S-glutathionylation intermediate. The question of why GRX-assisted glutathione-dependent catalysis evolved [68,85] is still open, especially regarding the plastid stroma. The main difference of mutants lacking class I GRX in comparison to mutants lacking GR may be that there is still sufficiently high GSH (and sufficiently low GSSG) for GSH-dependent (GRX-independent) reduction. In absence of class I GRX activity, reduction of disulfides still occurs, but at lower rates driven by thermodynamics (Fig. 8).

In conclusion, the most likely class I GRX functions remain thiol protection and enzyme regulation in response to oxidative challenge [26,86]. Potentially, fast kinetic equilibration with E_{GSH} is just relevant for enzymes with an S-glutathionylation intermediate on catalytic cysteines, as they would be temporarily “locked” in their disulfide or -SSG form in absence of a class I GRX. In the stroma, 1Cys methionine sulfide reductase B1 and peroxiredoxin IIE are interesting candidates [87,

88]. Alternatively, protein Cys with low pK_a could have evolved on proteins involved in (moonlighting) signalling functions in response to oxidative challenge, which still await identification as specific GRX interaction partners.

Author contributions

FB, MZ, PT, AJM and SJM-S designed the research. FB, JR, SST, HJ, FR, AB, SB, OT, MS, SK performed experiments and analysed data. SJM-S, MSchw., AJM, PJ, MD, EN, MZ, PT supervised the research and provided resources.

FB and SJMS wrote the manuscript with contributions from all authors. All authors approved the manuscript before submission.

Declaration of competing interest

The authors declare that they have no known competing financial interests or personal relationships that could have appeared to influence the work reported in this paper.

Data availability

Data will be made available on request.

Acknowledgements

We thank Andreas Werle-Rutter (Molecular Botany RPTU), Maria Homagk (Chemical Signalling, INRES, University of Bonn) and Bastian Welter (University of Cologne) for technical assistance, as well as Prof. Frank Hochholdinger for support. We thank Dr. Marlene Elsässer and Dr. Mareike Schallenberg-Rüdinger for generating a Gateway version of the *PTA2_Act5* expression vector.

This work was supported by the DFG-funded Research Training Group GRK2064: ‘Water use efficiency and drought stress responses: From Arabidopsis to Barley’ (AJM, MSchw., FB and SJM-S) and via the Joint Mobility Program between the DAAD (PPP Italy 57397466) and the MIUR (Prog. n. 34433) (AJM and PT). JR was supported by a PhD grant from the University of Bologna (PhD programs in Cellular Molecular Biology). Research in SK’s laboratory is funded by DFG under Germany’s Excellence Strategy –EXC 2048/1 – project 390686111. SJM-S and OT are grateful for funding obtained from BioComp 3.0 ‘Dynamic Membrane Processes in Biological Systems’. HJ, ST and SJM-S are grateful for support by the DFG-funded Research Training Group GRK2737 ‘STRESSistance’.

Appendix A. Supplementary data

Supplementary data to this article can be found online at <https://doi.org/10.1016/j.redox.2023.103015>.

References

- [1] M. Schreiber, S.A. Rensing, S.B. Gould, The greening ashore, *Trends Plant Sci.* 27 (2022) 847–857.
- [2] T. Roach, A. Krieger-Liszczay, Regulation of photosynthetic electron transport and photoinhibition, *Curr. Protein Pept. Sci.* 15 (2014) 351–362.
- [3] M.A. Schöttler, S.Z. Toth, Photosynthetic complex stoichiometry dynamics in higher plants: environmental acclimation and photosynthetic flux control, *Front. Plant Sci.* 5 (2014) 188.
- [4] A. Alboresi, M. Storti, T. Morosinotto, Balancing protection and efficiency in the regulation of photosynthetic electron transport across plant evolution, *New Phytol.* 221 (2019) 105–109.
- [5] A. Morales, E. Kaiser, Photosynthetic acclimation to fluctuating irradiance in plants, *Front. Plant Sci.* 11 (2020) 268.
- [6] B.B. Buchanan, A. Holmgren, J.-P. Jacquot, R. Scheibe, Fifty years in the thioredoxin field and a bountiful harvest, *Biochim Biophys Acta BBA - Gen Subj* 1820 (2012) 1822–1829.
- [7] B.B. Buchanan, Y. Balmer, Redox regulation: a broadening horizon, *Annu. Rev. Plant Biol.* 56 (2005) 187–220.

- [8] M. Balsera, E. Uberegui, P. Schürmann, B.B. Buchanan, Evolutionary development of redox regulation in chloroplasts, *Antioxidants Redox Signal.* 21 (2014) 1327–1355.
- [9] L. Marri, G. Thieulin-Pardo, R. Lebrun, R. Puppo, M. Zaffagnini, P. Trost, B. Gontero, F. Sparla, CP12-mediated protection of Calvin-Benson cycle enzymes from oxidative stress, *Biochimie* 97 (2014) 228–237.
- [10] L. Michelet, M. Zaffagnini, S. Morisse, F. Sparla, M.E. Pérez-Pérez, F. Francia, A. Danon, C.H. Marchand, S. Fermi, P. Trost, et al., Redox regulation of the Calvin-Benson cycle: something old, something new, *Front. Plant Sci.* 4 (2013) 470.
- [11] D.D. Gütle, T. Roret, S.J. Müller, J. Couturier, S.D. Lemaire, A. Hecker, T. Dhalleine, B.B. Buchanan, R. Reski, O. Einsle, et al., Chloroplast FBPase and SBPase are thioredoxin-linked enzymes with similar architecture but different evolutionary histories, *Proc. Natl. Acad. Sci. U. S. A.* 113 (2016) 6779–6784.
- [12] L. Gurrieri, F. Sparla, M. Zaffagnini, P. Trost, Dark complexes of the Calvin-Benson cycle in a physiological perspective, *Semin. Cell Dev. Biol.* S1084–9521 (23) (2023) 00049–6.
- [13] P. Geigenberger, I. Thormählen, D.M. Daloso, A.R. Fernie, The unprecedented versatility of the Plant thioredoxin system, *Trends Plant Sci.* 22 (2017) 249–262.
- [14] D. Zimmer, C. Swart, A. Graf, S. Arrivault, M. Tillich, S. Proost, Z. Nikoloski, M. Stitt, R. Bock, T. Mühlhaus, et al., Topology of the redox network during induction of photosynthesis as revealed by time-resolved proteomics in tobacco, *Sci. Adv.* 7 (2021) eabi8307.
- [15] J.T. Teh, V. Leitz, V.J.C. Holzer, D. Neusius, G. Marino, T. Meitzel, J.G. García-Cerdán, R.M. Dent, K.K. Niyogi, P. Geigenberger, et al., NTRC regulates CP12 to activate Calvin-Benson cycle during cold acclimation, *Proc. Natl. Acad. Sci. U. S. A.* 120 (2023) e2306338120.
- [16] K. Yoshida, Y. Yokochi, T. Hisabori, New light on chloroplast redox regulation: molecular mechanism of protein thiol oxidation, *Front. Plant Sci.* 10 (2019) 1534.
- [17] J.M. Pérez-Ruiz, B. Naranjo, V. Ojeda, M. Guinea, F.J. Cejudo, NTRC-dependent redox balance of 2-Cys peroxidoredoxins is needed for optimal function of the photosynthetic apparatus, *Proc. Natl. Acad. Sci. U. S. A.* 114 (2017) 12069–12074.
- [18] V. Ojeda, J.M. Pérez-Ruiz, F.J. Cejudo, 2-Cys peroxidoredoxins participate in the oxidation of chloroplast enzymes in the dark, *Mol. Plant* 11 (2018) 1377–1388.
- [19] M.-J. Vaseghi, K. Chibani, W. Telman, M.F. Liebthal, M. Gerken, H. Schnitzer, S. M. Mueller, K.-J. Dietz, The chloroplast 2-cysteine peroxidoredoxin functions as thioredoxin oxidase in redox regulation of chloroplast metabolism, *Elife* 7 (2018) 38194.
- [20] M. Deponte, The incomplete glutathione puzzle: just guessing at numbers and figures? *Antioxidants Redox Signal.* 27 (2017) 1130–1161.
- [21] B. Alvarez, G. Salinas, Basic concepts of thiol chemistry and biology, *Redox Chem. Biol. Thiols* (2022) 1–18. Elsevier.
- [22] S.A.K. Bangash, S.J. Müller-Schüssele, D. Solbach, M. Jansen, F. Fiorani, M. Schwarzländer, S. Kopriva, A.J. Meyer, Low-glutathione mutants are impaired in growth but do not show an increased sensitivity to moderate water deficit, *PLoS One* 14 (2019) e0220589.
- [23] C. Cassier-Chauvat, F. Marceau, S. Farci, S. Ouchane, F. Chauvat, The glutathione system: a journey from cyanobacteria to higher eukaryotes, *Antioxid Basel Switz* 12 (2023) 1199.
- [24] G. Noctor, A. Mhamdi, S. Chaouch, Y. Han, J. Neukermans, B. Marquez-Garcia, G. Queval, C.H. Foyer, Glutathione in plants: an integrated overview: glutathione status and functions, *Plant Cell Environ.* 35 (2012) 454–484.
- [25] S.J. Müller-Schüssele, F. Bohle, J. Rossi, P. Trost, A.J. Meyer, M. Zaffagnini, Plasticity in plastid redox networks: evolution of glutathione-dependent redox cascades and glutathionylation sites, *BMC Plant Biol.* 21 (2021) 322.
- [26] A.P. Fernandes, A. Holmgren, Glutaredoxins: glutathione-dependent redox enzymes with functions far beyond a simple thioredoxin backup system, *Antioxidants Redox Signal.* 6 (2004) 63–74.
- [27] C.H. Lillig, C. Berndt, A. Holmgren, Glutaredoxin systems, *Biochim Biophys Acta BBA - Gen Subj* 1780 (2008) 1304–1317.
- [28] J. Couturier, J.-P. Jacquot, N. Rouhier, Toward a refined classification of class I dithiol glutaredoxins from poplar: biochemical basis for the definition of two subclasses, *Front. Plant Sci.* 4 (2013) 518.
- [29] D. Trnka, A.D. Engelke, M. Gellert, A. Moseler, M.F. Hossain, T.T. Lindenberg, L. Pedroletti, B. Odermatt, J.V. de Souza, A.K. Bronowska, et al., Molecular basis for the distinct functions of redox-active and FeS-transferring glutaredoxins, *Nat. Commun.* 11 (2020) 3445.
- [30] D.P. Dixon, R. Edwards, Glutathione transferases, *Arabidopsis Book* 8 (2010) e0131.
- [31] N.A. Rashdan, B. Shrestha, C.B. Pattillo, S-glutathionylation, friend or foe in cardiovascular health and disease, *Redox Biol.* 37 (2020) 101693.
- [32] L. Michelet, M. Zaffagnini, C. Marchand, V. Collin, P. Decottignies, P. Tsan, J.-M. Lancelin, P. Trost, M. Miginiac-Maslow, G. Noctor, et al., Glutathionylation of chloroplast thioredoxin f is a redox signaling mechanism in plants, *Proc. Natl. Acad. Sci. USA* 102 (2005) 16478–16483.
- [33] M. Zaffagnini, L. Michelet, C. Marchand, F. Sparla, P. Decottignies, P. Le Maréchal, M. Miginiac-Maslow, G. Noctor, P. Trost, S.D. Lemaire, The thioredoxin-independent isoform of chloroplastic glyceraldehyde-3-phosphate dehydrogenase is selectively regulated by glutathionylation, *FEBS J.* 274 (2007) 212–226.
- [34] M. Bedhomme, M. Zaffagnini, C.H. Marchand, X.-H. Gao, M. Moslonka-Lefebvre, L. Michelet, P. Decottignies, S.D. Lemaire, Regulation by glutathionylation of isocitrate lyase from *Chlamydomonas reinhardtii*, *J. Biol. Chem.* 284 (2009) 36282–36291.
- [35] M. Zaffagnini, S. Fermi, A. Costa, S.D. Lemaire, P. Trost, Plant cytoplasmic GAPDH: redox post-translational modifications and moonlighting properties, *Front. Plant Sci.* 4 (2013) 450.
- [36] T. Draculic, I.W. Dawes, C.M. Grant, A single glutaredoxin or thioredoxin gene is essential for viability in the yeast *Saccharomyces cerevisiae*, *Mol. Microbiol.* 36 (2000) 1167–1174.
- [37] X. Yu, T. Pasternak, M. Eiblmeier, F. Ditengou, P. Kochersperger, J. Sun, H. Wang, H. Rennenberg, W. Teale, I. Paponov, et al., Plastid-localized glutathione reductase-2-regulated glutathione redox status is essential for Arabidopsis root apical meristem maintenance, *Plant Cell* 25 (2013) 4451–4468.
- [38] M. Schwarzländer, T.P. Dick, A.J. Meyer, B. Morgan, Dissecting redox biology using fluorescent protein sensors, *Antioxidants Redox Signal.* 24 (2016) 680–712.
- [39] L. Marty, D. Bausewein, C. Müller, S.A.K. Bangash, A. Moseler, M. Schwarzländer, S.J. Müller-Schüssele, B. Zechmann, C. Riondet, J. Balk, et al., Arabidopsis glutathione reductase 2 is indispensable in plastids, while mitochondrial glutathione is safeguarded by additional reduction and transport systems, *New Phytol.* 224 (2019) 1569–1584.
- [40] S.J. Müller-Schüssele, R. Wang, D.D. Gütle, J. Romer, M. Rodriguez-Franco, M. Scholz, F. Buchert, V.M. Lüth, S. Kopriva, P. Dörmann, et al., Chloroplasts require glutathione reductase to balance reactive oxygen species and maintain efficient photosynthesis, *Plant J.* 103 (2020) 1140–1154.
- [41] A.J. Meyer, T. Brach, L. Marty, S. Kreye, N. Rouhier, J.-P. Jacquot, R. Hell, Redox-sensitive GFP in *Arabidopsis thaliana* is a quantitative biosensor for the redox potential of the cellular glutathione redox buffer, *Plant J.* 52 (2007) 973–986.
- [42] M. Gutscher, A.-L. Pauleau, L. Marty, T. Brach, G.H. Wabnitz, Y. Samstag, A. J. Meyer, T.P. Dick, Real-time imaging of the intracellular glutathione redox potential, *Nat. Methods* 5 (2008) 553–559.
- [43] M. Schwarzländer, M.D. Fricker, C. Müller, L. Marty, T. Brach, J. Novak, L. J. Sweetlove, R. Hell, A.J. Meyer, Confocal imaging of glutathione redox potential in living plant cells, *J. Microsc.* 231 (2008) 299–316.
- [44] Z. Haber, N. Lampl, A.J. Meyer, E. Zelinger, M. Hipsch, S. Rosenwasser, Resolving diurnal dynamics of the chloroplastic glutathione redox state in Arabidopsis reveals its photosynthetically derived oxidation, *Plant Cell* 33 (2021) 1828–1844.
- [45] L. Marty, W. Siala, M. Schwarzländer, M.D. Fricker, M. Wirtz, L.J. Sweetlove, Y. Meyer, A.J. Meyer, J.-P. Reichheld, R. Hell, The NADPH-dependent thioredoxin system constitutes a functional backup for cytosolic glutathione reductase in Arabidopsis, *Proc. Natl. Acad. Sci. USA* 106 (2009) 9109–9114.
- [46] J. Couturier, E. Ströher, A.-N. Albetel, T. Roret, M. Muthuramalingam, L. Tarrago, T. Seidel, P. Tsan, J.-P. Jacquot, M.K. Johnson, et al., Arabidopsis chloroplastic glutaredoxin C5 as a model to explore molecular determinants for iron-sulfur cluster binding into glutaredoxins, *J. Biol. Chem.* 286 (2011) 27515–27527.
- [47] A.J. Meyer, A. Dreyer, J.M. Ugalde, E. Feitosa-Araujo, K.-J. Dietz, M. Schwarzländer, Shifting paradigms and novel players in Cys-based redox regulation and ROS signaling in plants - and where to go next, *Biol. Chem.* 402 (2021) 399–423.
- [48] N. Rouhier, H. Unno, S. Bandyopadhyay, L. Masip, S.-K. Kim, M. Hirasawa, J. M. Gualberto, V. Lattard, M. Kusunoki, D.B. Knaff, et al., Functional, structural, and spectroscopic characterization of a glutathione-ligated [2Fe–2S] cluster in poplar glutaredoxin C1, *Proc. Natl. Acad. Sci. USA* 104 (2007) 7379–7384.
- [49] J.M. Ugalde, P. Fuchs, T. Nietzel, E.A. Cutolo, M. Homagk, U.C. Vothknecht, L. Holuigue, M. Schwarzländer, S.J. Müller-Schüssele, A.J. Meyer, Chloroplast-derived photo-oxidative stress causes changes in H₂O₂ and E_{CSH} in other subcellular compartments, *Plant Physiol* 186 (2021) 125–141.
- [50] M. Zaffagnini, L. Michelet, V. Massot, P. Trost, S.D. Lemaire, Biochemical characterization of glutaredoxins from *Chlamydomonas reinhardtii* reveals the unique properties of a chloroplastic CGFs-type glutaredoxin, *J. Biol. Chem.* 283 (2008) 8868–8876.
- [51] M.M. Bradford, A rapid and sensitive method for the quantitation of microgram quantities of protein utilizing the principle of protein-dye binding, *Anal. Biochem.* 72 (1976) 248–254.
- [52] F. Bohle, A.J. Meyer, S.J. Müller-Schüssele, Quantification of redox-sensitive GFP cytosine redox state via gel-based read-out, in: M. Sharma (Ed.), *Fluoresc. Proteins*, Springer US, New York, NY, 2023, pp. 259–268.
- [53] R. Reski, W.O. Abel, Induction of budding on chloronemata and caulonemata of the moss, *Physcomitrella patens*, using isopentenyladenine, *Planta* 165 (1985) 354–358.
- [54] G.-W. Tian, A. Mohanty, S.N. Chary, S. Li, B. Paap, G. Drakakaki, C.D. Kopec, J. Li, D. Ehrhardt, D. Jackson, et al., High-throughput fluorescent tagging of full-length Arabidopsis gene products in planta, *Plant Physiol* 135 (2004) 25–38.
- [55] A. Hohe, T. Egner, J.M. Lucht, H. Holtorf, C. Reinhard, G. Schween, R. Reski, An improved and highly standardised transformation procedure allows efficient production of single and multiple targeted gene-knockouts in a moss, *Physcomitrella patens*, *Curr. Genet.* 44 (2004) 339–347.
- [56] A. Speiser, M. Silbermann, Y. Dong, S. Haberland, V.V. Uslu, S. Wang, S.A. K. Bangash, M. Reichelt, A.J. Meyer, M. Wirtz, et al., Sulfur partitioning between glutathione and protein synthesis determines plant growth, *Plant Physiol* 177 (2018) 927–937.
- [57] M. Kubo, A. Imai, T. Nishiyama, M. Ishikawa, Y. Sato, T. Kurata, Y. Hiwatashi, R. Reski, M. Hasebe, System for stable β-estradiol-inducible gene expression in the moss *Physcomitrella patens*, *PLoS One* 8 (2013) e77356.
- [58] S.J. Müller, R. Reski, Mitochondrial dynamics and the ER: the plant perspective, *Front. Cell Dev. Biol.* 3 (2015) 78.
- [59] S.J. Müller, D. Lang, S.N.W. Hoernstein, E.G.E. Lang, C. Schüssele, A. Schmidt, M. Fluck, D. Leisbach, C. Niegler, A.D. Zimmer, et al., Quantitative analysis of the mitochondrial and plastid proteomes of the moss *Physcomitrella patens* reveals protein macrocompartmentation and microcompartmentation, *Plant Physiol* 164 (2014) 2081–2095.
- [60] M.D. Fricker, Quantitative redox imaging software, *Antioxidants Redox Signal.* 24 (2016) 752–762.

- [61] I. Aller, N. Rouhier, A.J. Meyer, Development of roGFP2-derived redox probes for measurement of the glutathione redox potential in the cytosol of severely glutathione-deficient *rml1* seedlings, *Front. Plant Sci.* 4 (2013) 506.
- [62] S. Wagner, J. Steinbeck, P. Fuchs, S. Lichtenauer, M. Elsässer, J.H.M. Schippers, T. Nietzel, C. Ruberti, O. Van Aken, A.J. Meyer, et al., Multiparametric real-time sensing of cytosolic physiology links hypoxia responses to mitochondrial electron transport, *New Phytol.* 224 (2019) 1668–1684.
- [63] D. Wessel, U.I. Flüge, A method for the quantitative recovery of protein in dilute solution in the presence of detergents and lipids, *Anal. Biochem.* 138 (1984) 141–143.
- [64] P. Begas, V. Staudacher, M. Deponte, Systematic re-evaluation of the bis(2-hydroxyethyl) disulfide (HEDS) assay reveals an alternative mechanism and activity of glutaredoxins, *Chem. Sci.* 6 (2015) 3788–3796.
- [65] P. Begas, L. Liedgens, A. Moseler, A.J. Meyer, M. Deponte, Glutaredoxin catalysis requires two distinct glutathione interaction sites, *Nat. Commun.* 8 (2017) 14835.
- [66] J. Couturier, C.S. Koh, M. Zaffagnini, A.M. Winger, J.M. Gualberto, C. Corbier, P. Decottignies, J.-P. Jacquot, S.D. Lemaire, C. Didierjean, et al., Structure-function relationship of the chloroplastic glutaredoxin S12 with an atypical WCSYS active site, *J. Biol. Chem.* 284 (2009) 9299–9310.
- [67] M. Zaffagnini, M. Bedhomme, C.H. Marchand, J.R.M. Couturier, X.-H. Gao, N. Rouhier, P. Trost, S.P.D. Lemaire, Glutaredoxin S12: unique properties for redox signaling, *Antioxidants Redox Signal.* 16 (2012) 17–32.
- [68] M. Deponte, Glutathione and glutathione-dependent enzymes, *Redox Chem. Biol. Thiols* (2022) 241–275. Elsevier.
- [69] A.J. Meyer, T.P. Dick, Fluorescent protein-based redox probes, *Antioxidants Redox Signal.* 13 (2010) 621–650.
- [70] E. Eckers, M. Bien, V. Stroobant, J.M. Herrmann, M. Deponte, Biochemical characterization of dithiol glutaredoxin 8 from *Saccharomyces cerevisiae*: the catalytic redox mechanism redux, *Biochemistry* 48 (2009) 1410–1423.
- [71] M. Zaffagnini, M. Bedhomme, C.H. Marchand, S. Morisse, P. Trost, S.D. Lemaire, Redox regulation in photosynthetic organisms: focus on glutathionylation, *Antioxidants Redox Signal.* 16 (2012) 567–586.
- [72] C. Riondet, J.P. Desouris, J.G. Montoya, Y. Chartier, Y. Meyer, J.-P. Reichheld, A dicotyledon-specific glutaredoxin GRXC1 family with dimer-dependent redox regulation is functionally redundant with GRXC2, *Plant Cell Environ.* 35 (2012) 360–373.
- [73] C.T. Dooley, T.M. Dore, G.T. Hanson, W.C. Jackson, S.J. Remington, R.Y. Tsien, Imaging dynamic redox changes in mammalian cells with green fluorescent protein indicators, *J. Biol. Chem.* 279 (2004) 22284–22293.
- [74] S.J. Müller-Schüssele, M. Schwarzländer, A.J. Meyer, Live monitoring of plant redox and energy physiology with genetically encoded biosensors, *Plant Physiol* 186 (2021) 93–109.
- [75] M. Schlößer, A. Moseler, Y. Bodnar, M. Homagk, S. Wagner, L. Pedroletti, M. Gellert, J.M. Ugalde, C.H. Lillig, A.J. Meyer, Localization of four class I glutaredoxins in the cytosol and the secretory pathway and characterization of their biochemical diversification, *bioRxiv* (2023), <https://doi.org/10.1101/2023.09.01.555924>.
- [76] S. Luikenhuis, G. Perrone, I.W. Dawes, C.M. Grant, The yeast *Saccharomyces cerevisiae* contains two glutaredoxin genes that are required for protection against reactive oxygen species, *Mol. Biol. Cell* 9 (1998) 1081–1091.
- [77] J. Zimmermann, J. Oestreich, S. Hess, J.M. Herrmann, M. Deponte, B. Morgan, One cysteine is enough: a monothiol Grx can functionally replace all cytosolic Trx and dithiol Grx, *Redox Biol.* 36 (2020) 101598.
- [78] F. Bohle, A. Klaus, H. Tegethof, M. Schwarzländer, F. Hochholdinger, A.J. Meyer, I. F. Acosta, S.J. Müller-Schüssele, High robustness of cytosolic glutathione redox potential under combined salt and osmotic stress in barley as revealed by the biosensor Grx1-roGFP2, *bioRxiv* (2022), <https://doi.org/10.1101/2022.12.22.521445>.
- [79] Y. Bodnar, M. Gellert, F.M. Hossain, C.H. Lillig, Breakdown of *Arabidopsis thaliana* thioredoxins and glutaredoxins based on electrostatic similarity—Leads to common and unique interaction partners and functions, *PLoS One* 18 (2023) e0291272.
- [80] W. Telman, M. Liebthal, K.-J. Dietz, Redox regulation by peroxiredoxins is linked to their thioredoxin-dependent oxidase function, *Photosynth. Res.* 145 (2020) 31–41.
- [81] M. Zaffagnini, S. Fermani, C.H. Marchand, A. Costa, F. Sparla, N. Rouhier, P. Geigenberger, S.D. Lemaire, P. Trost, Redox homeostasis in photosynthetic organisms: novel and established thiol-based molecular mechanisms, *Antioxidants Redox Signal.* 31 (2019) 155–210.
- [82] P. Trost, S. Fermani, M. Calvaresi, M. Zaffagnini, Biochemical basis of sulphenomics: how protein sulphenic acids may be stabilized by the protein microenvironment, *Plant Cell Environ.* 40 (2017) 483–490.
- [83] D. Talwar, C.G. Miller, J. Grossmann, L. Szyrwiel, T. Schwewecke, V. Demichev, A.-M. Mikecin Drazic, A. Mayakonda, P. Lutsik, C. Veith, et al., The GAPDH redox switch safeguards reductive capacity and enables survival of stressed tumor cells, *Nat. Metab.* 5 (2023) 660–676.
- [84] M. Zaffagnini, C.H. Marchand, M. Malferrari, S. Murail, S. Bonacchi, D. Genovese, M. Montalti, G. Venturoli, G. Falini, M. Baaden, et al., Glutathionylation primes soluble glyceraldehyde-3-phosphate dehydrogenase for late collapse into insoluble aggregates, *Proc. Natl. Acad. Sci. USA* 116 (2019) 26057–26065.
- [85] M. Deponte, Glutathione catalysis and the reaction mechanisms of glutathione-dependent enzymes, *Biochim Biophys Acta BBA - Gen Subj* 1830 (2013) 3217–3266.
- [86] C. Berndt, C.H. Lillig, L. Flohé, Redox regulation by glutathione needs enzymes, *Front. Pharmacol.* 5 (2014) 168.
- [87] F. Gama, C. Bréhélin, E. Gelhaye, Y. Meyer, J.-P. Jacquot, P. Rey, N. Rouhier, Functional analysis and expression characteristics of chloroplastic Prx IIE, *Physiol. Plantarum* 133 (2008) 599–610.
- [88] E. Laugier, L. Tarrago, C. Vieira Dos Santos, F. Eymery, M. Havaux, P. Rey, *Arabidopsis thaliana* plastidial methionine sulfoxide reductases B, MSRBs, account for most leaf peptide MSR activity and are essential for growth under environmental constraints through a role in the preservation of photosystem antennae, *Plant J.* 61 (2009) 271–282.